

# Kif9 is an active kinesin motor required for ciliary beating and proximodistal patterning of motile axonemes

Mia J. Konjikusic<sup>1,2,3</sup>, Chanjae Lee<sup>1</sup>, Yang Yue<sup>4</sup>, Bikram D. Shrestha<sup>5</sup>, Ange M. Nguimtsop<sup>1</sup>, Amjad Horani<sup>6</sup>, Steven Brody<sup>7,8</sup>, Vivek N. Prakash<sup>5,9</sup>, Ryan S. Gray<sup>2,3</sup>, Kristen J. Verhey<sup>4</sup>, John B. Wallingford<sup>1\*</sup>

<sup>1</sup> Department of Molecular Biosciences, University of Texas at Austin, Austin, TX, USA.

<sup>2</sup> Department of Pediatrics, Dell Pediatric Research Institute, 1400 Barbara Jordan Blvd, The University of Texas at Austin, Dell Medical School, Austin, TX, USA.

<sup>3</sup> Department of Nutritional Sciences, 200 W 24<sup>th</sup> Street, The University of Texas at Austin, Austin, TX 78712, USA.

<sup>4</sup> Department of Cell and Developmental Biology, University of Michigan Medical School, Ann Arbor, MI, 48109, USA.

<sup>5</sup> Department of Physics, University of Miami, Coral Gables, FL, USA.

<sup>6</sup> Department of Pediatrics, Washington University School of Medicine, St. Louis, MO, USA.

<sup>7</sup> Department of Medicine, Washington University School of Medicine, St. Louis, MO, USA.

<sup>8</sup> Department of Cell Biology and Physiology, Washington University School of Medicine, St. Louis, MO, 63110 USA

<sup>9</sup> Department of Biology and Department of Marine Biology and Ecology, University of Miami, Coral Gables, FL, USA.

\*Corresponding Author: Wallingford@austin.utexas.edu

Patterson Labs  
2401 Speedway  
Austin, Tx 78712

## Abstract:

Most motile cilia have a stereotyped structure of nine microtubule outer doublets and a single central pair of microtubules. The central pair microtubules are surrounded by a set of proteins, termed the central pair apparatus. A specific kinesin, Klp1 projects from the central pair and contributes to ciliary motility in *Chlamydomonas*. The vertebrate orthologue, Kif9 is required for beating in mouse sperm flagella, but the mechanism of Kif9/Klp1 function remains poorly defined. Here, using *Xenopus* epidermal multiciliated cells, we show that Kif9 is necessary for ciliary motility and the proper distal localization of not only central pair proteins, but also radial spokes and dynein arms. In addition, single-molecule assays *in vitro* revealed that *Xenopus* Kif9 is a long-range processive motor, though it does not perform long-range movement in ciliary axonemes *in vivo*. Together, our data suggest that Kif9 is integral for ciliary beating and is necessary for proper axonemal distal end integrity.

## Introduction:

Motile cilia are essential for fluid flow across epithelia and for cell motility in a variety of contexts in the animal kingdom (Brooks and Wallingford, 2014; Spassky and Meunier, 2017; Ishikawa, 2017). Most motile cilia have a conserved radial structure of nine microtubule outer doublets and a single central pair of microtubules. Ciliary motility relies on several different protein complexes that are organized throughout the axoneme in a specific fashion. These include the inner and outer dynein arms on the outer microtubule doublets and radial spokes that connect to inner dynein arms and project towards to central pair (Ishikawa, 2017). In addition, studies indicate that ~50 different proteins surround the central pair to form the central pair apparatus (CA) (Loreng and Smith, 2017; Dai et al., 2020; Zhao et al., 2019). More recent studies on the structure of the active central pair highlight the role of a specific Kinesin, Klp1 in *Chlamydomonas* or Kif9 in vertebrates, in beating and ciliary waveform through the central pair

(Han et al., 2022). All of these elements work in concert to orchestrate proper ciliary beat frequency and waveform.

In addition to the radial patterning of motile axonemes, a complex proximal to distal patterning has been extensively studied in *Chlamydomonas* and *Tetrahymena* (Pedersen et al., 2003; Bui et al., 2012; Louka et al., 2018). Though less well-defined, such proximodistal patterning is also critical in vertebrate multiciliated cells (Fliegau et al., 2005; Loges et al., 2008; Yamamoto et al., 2010). The function and composition of the distal tip of motile cilia is of particular interest, as it is thought to be critical to protect the axoneme from disintegration due to the massive forces associated with beating. The distal tip differs in structure widely across ciliary types (Soares et al., 2019), but enrichment of the microtubule end-binding proteins Eb1 and Eb3 in distal regions is conserved from algae to vertebrates (Brooks and Wallingford, 2012; Schröder et al., 2011; Pedersen et al., 2003). Additionally, we and others have identified Spef1, a microtubule bundling protein, is also highly enriched in the distal tip of motile axonemes in *Xenopus* (Gray et al., 2009; Schröder et al., 2011, 1). Interestingly, Spef1 also contributes to central pair formation in mouse multiciliated cells. Whether Spef1 and the central apparatus contribute to tip integrity in multiciliated cells remains unclear.

Here, we examined the function of Kif9, the vertebrate homolog of the *Chlamydomonas* kinesin Klp1, which projects from the C2 microtubule of the central pair and is required for ciliary beating (Bernstein et al., 1994, 1; Miyata et al., 2020; Yokoyama et al., 2004; Lechtreck and Witman, 2007). A recent report describes improper waveforms and disrupted ciliary beat in sperm from Kif9 mutant mice (Miyata et al., 2020), and as in *Chlamydomonas*, Kif9 mutant sperm do not display overt defects in the assembly of the central pair microtubules (Yokoyama et al., 2004; Miyata et al., 2020). Thus, the mechanisms by which loss of Klp1/Kif9 disrupts cilia beating remain unclear.

Recently a study Cryo-EM structure of the active central pair apparatus in *Chlamydomonas* shows that Klp1, does not participate in long-range transport along microtubules, but instead is stably bound to the central pair C2 microtubule and produces 16nm swings between ATP bound states (Han et al., 2022). This result further suggests Kif9 is necessary for ciliary beating in a manner similar to that of axonemal dyneins, not using its motor for trafficking of cargo but instead for of beating. Here, we find that loss of the vertebrate ortholog of Klp1, Kif9 in *Xenopus* results in defects in ciliary beating and cilia length related to specific disruption of the distal tip of the axoneme. Strikingly, we observed loss not only of central pair proteins, but also of radial spokes and dynein arms from distal axonemes after Kif9 knockdown. Finally, we show that Kif9 is a slowly processive microtubule motor *in vitro* though it displays only negligible long-range movement in the axoneme. These data provide new insights into the central pair contribution to ciliary beating and so may contribute to our understanding of human motile ciliopathies.

## Results:

### **Kif9 localizes to the axonemes of multiciliated cells in *Xenopus* and human airways.**

*Xenopus* tadpoles are a powerful model for studying the formation and function of multiciliated cells (Walentek and Quigley, 2017), so we used this system to examine the localization of Kif9 in multiciliated cells. *En face* confocal imaging of Kif9-GFP mRNA-injected, whole mounted embryos revealed localization to cilia and basal bodies of multiciliated cells (Figure 1A-B”). We confirmed endogenous Kif9 localization in ciliary axonemes using immunofluorescence and co-staining with acetylated tubulin (Figure 1C-C”). This localization is also evolutionarily conserved, as Kif9 immunostaining of human airway MCCs also revealed localization to cilia (Figure 1F-F”). Thus, Kif9 is expressed in *Xenopus* and human airway multiciliated cells where it localizes to ciliary axonemes.

### **Kif9 is necessary for ciliary beating in multiciliated cells.**

Multiciliated cells generate fluid flow across several different epithelia (Brooks and Wallingford, 2014; Spassky and Meunier, 2017) and the *Xenopus* epidermis offers an accessible model for studying those flows (Walentek and Quigley, 2017). In order to knockdown (KD) expression of Kif9 and study effects of its loss on cilia-mediated fluid flow, we designed a splice-blocking morpholino oligonucleotides against the first exon of Kif9 in *Xenopus*. Kif9 mRNA knockdown was confirmed by RT-PCR (Supp. Figure 1A). Crucially, imaging of Kif9 immunostaining in knockdown cilia also revealed reduced levels of Kif9 protein in cilia (Figure 1D-D", 1E).

To visualize flows, we whole mounted embryos with beads mixed into the media and imaged at high speeds with confocal microscopy. Using Flowtrace analysis (Gilpin et al., 2017), we highlighted tracks created by beads across frames (Movie 1, 2 and 3). We then used Particle Image Velocimetry (PIV) analysis to quantify the ciliary beating-induced fluid flow speeds. In control embryos, we observed average fluid flow speeds of about 154 microns/second, whereas morpholino injected embryos showed a ten-fold reduction in flow (P-value = 0.0094; Figure 2A-B, 2D). Reintroduction of Kif9-GFP mRNA into knockdown embryos rescued the flow defects, restoring flow rates to ~42 microns/second, thereby supporting the specificity of this phenotype (Figure 2C-2D, P-value = 0.0280).

To ask how Kif9 knockdown affects ciliary beating, we used high-speed imaging of cilia labeled with a CAAX-GFP (membrane-GFP; Movies 4, 5, 6). Compared to controls, Kif9 KD embryos displayed beat defects that were restored in the rescued embryos (Figure 2E-F). These beat defects ranged from complete paralysis of cilia, to reduced beat frequency and disrupted waveforms. We also frequently observed cilia that stall during their beat cycle (Figure 2F-F"" black arrowheads).

Kymographs further highlight the deficiencies in Kif9 knockdown embryos, including revealing the irregular beat (Fig. 2G, H). Both the speed and regularity of beating was restored in rescued embryos (Figure 2I). Quantification revealed a mean beat frequency of ~37 Hz for controls, and this was reduced by half in Kif9 knockdowns, with cells displaying a bimodal distribution of speeds (some paralyzed, other with reduced beat frequencies). Notably, even those cilia that do beat do so more slowly (Fig. 2J). In rescue embryos ciliary beat was restored to 34.02 Hz (p-value<0.0001) (Figure 2J).

Finally, in addition to ciliary beat defects, Kif9 KD embryos also had shorter cilia than controls (P-value < 0.0001, Figure 2L-M, 2O). This phenotype was also rescued by expression of Kif9-GFP (P-value = 0.0174; Figure 2N, 2O). These findings are consistent with the finding that axoneme length is often affected in central pair mutants in *Chlamydomonas* (Lechtreck et al., 2013). Together, these data demonstrate that Kif9 is necessary for normal ciliary length and beating in vertebrate multiciliated cells.

### **Kif9 is necessary for central pair protein localization along the proximal/distal axis of the axoneme.**

We wished to assess how loss of Kif9 affects other components of the central pair. We first considered Fap266, as proteomic data in *Chlamydomonas* suggest this central pair protein may interact with Klp1/Kif9 (Dai et al., 2020; Zhao et al., 2019). The vertebrate orthologue of Fap266 has not been established, but Rsph10b is the most likely candidate and a recent paper demonstrated that Rsph10b is *not* present in mouse radial spokes further suggesting it may be a central pair protein (Zheng et al., 2021). We therefore generated a GFP fusions to Rsph10b and found that its normal axonemal localization was disrupted after Kif9 KD (Figure 3B-C').

Intriguingly, this defect was restricted to the distal ends of the cilia (Figure 3B-E). Live confocal imaging of embryos injected with membrane-RFP (gray) and GFP-Rsph10b (orange) revealed a striking reduction in localization of Rsph10b in the distal axoneme. This loss was not simply a consequence of reduced cilia length, as we measured the length of cilia containing

Rsph10b protein and normalized it to total cilia length as indicated by membrane-RFP; this quantification revealed that the proportion of the cilium occupied by Rsph10b was reduced (Figure 3F). Moreover, when we quantified fluorescence intensity along individual axonemes, we observed that fluorescence intensity of Rsph10b was increased in the proximal regions of Kif9 KD axonemes (Supp. Figure 2E)

Because the exact orthology of Rsph10b/Fap266 remains poorly defined, we next examined bona fide vertebrate central apparatus proteins. Kif9/Klp1 is present in the C2 region of the central apparatus, and we found that the C2 “bridge” protein Spag16 (Pf20 in *Chlamydomonas*) was also lost specifically from the distal axonemes (Figure 3G-J). So too was the C1-associated ciliopathy protein Cfap74 (Dai et al., 2020; Zhao et al., 2019; Sha et al., 2020)(Figure 3L-P, Supp. Figure 2C-D). However, unlike Rsph10b, neither Spag16 nor Cfap74 was increased in the proximal axonemes (Supp. Figure 2B,D,F). Together, these data suggest that loss of Kif9 leads to complex alterations in CA protein localization in motile cilia.

### **Loss of Kif9 affects the proximal to distal patterning of Radial Spokes, Inner Dynein Arms and Outer Dynein Arms in the cilium.**

Previous studies suggest, but have not demonstrated, links between the Kif9/Klp1 and radial spokes in *Chlamydomonas* (Yokoyama, 2004; Lechtrek, 2007). We therefore examined the localization of Nme5/Rsph23, a radial spoke stalk or “neck” protein that is out of direct contact from the central pair apparatus (Cho et al., 2020). Live confocal imaging of control and Kif9 KD embryos revealed a striking reduction in Rsph23 along the axonemes (Figure 4A-B’), stemming specifically from a loss of Rsph23 from the distal ends of the axonemes (Figure 4C-D, P-value = 0.0023, Supp. Figure 2G-H).

Radial Spoke proteins control the activity of axonemal dyneins, and radial spoke mutants in many species display paralyzed flagella (Viswanadha et al., 2017). We therefore asked if loss of Kif9 also affected inner and outer dynein arm localization in the axoneme by examining GFP-Dnali1 or GFP-Dnai1, respectively. Strikingly, we observed that both inner dynein arm Dnali1 and outer dynein arm Dnai1 were reduced in distal axonemes (Figure 4F-O).

### **Kif9 contributes to distal tip integrity in motile axonemes.**

The specific, distal loss of central apparatus, radial spoke, and axonemal dynein components led us to ask if Kif9 may contribute to the specialized structures of the axoneme distal tip (Soares et al., 2019). We therefore examined the localization of Spef1, a microtubule bundling protein that is both enriched in the distal tips of *Xenopus* multiciliated cilia and is required for central pair assembly in mammals (Gray et al., 2009; Chan et al., 2005; Zheng et al., 2019). First, we show that Spef1 does indeed localize to multiciliated cell ciliary tips in mouse tracheal and human airway multiciliated cells (Figure 5B-C’). This confirms our previous localization of Spef1 in frog multiciliated cells using RFP-Spef1 (Gray et al., 2009). Interestingly, when we looked at Kif9 and Spef1 localization in the tip, we found that unlike other beating machinery, Kif9 protein extended distally in the region marked by enriched Spef1. Unlike Spef1, however, Kif9 was not enriched in this region but rather displayed a mosaic, speckled pattern that was not consistent from cilium to cilium (Figure 5D-E”).

More importantly, by co-expressing RFP-Spef1 with membrane-GFP we observed a striking loss of the Spef1-enriched tip domain in Kif9 knockdown cilia (Figure 5F-G’). This phenotype was specific, as it was rescued by re-introduction of Kif9 mRNA (Figure 5H-H’). We quantified this loss using fluorescence intensity traces along the cilium (Figure 5I).

Finally, this phenotype did not reflect a general defect in the distal cilium tip, as other proteins that decorate this region were unaffected after Kif9 loss. For example, the microtubule plus-end binding protein Eb3 displays a broad distal enrichment similar to Spef1 (Figure 6),

while Eb1 displays a more concentrated enrichment at the extreme distal end of the cilium (Figure 6). Both Eb1 and Eb3 remained distally enriched after Kif9 loss. These data argue that Kif9 contributes to the localization of specific elements of the distal tip of motile axonemes.

### **Kif9 can bind microtubules and has slow processivity *in vitro* but displays negligible movement in axonemes.**

Kinesins play diverse cellular roles. While most kinesins acts as motors for intracellular trafficking, others function as microtubule associated proteins or microtubule depolymerizing proteins (Konjikusic et al., 2021). Klp1 binds microtubules *in vitro* (Yokoyama et al., 2004), but its motor activity and the microtubule interactions of its vertebrate ortholog, Kif9, remain unknown. We therefore turned to single-molecule motility assays to assess Kif9 and its behavior on microtubules. Full length *Xenopus* Kif9 showed no ability to bind microtubules *in vitro* (Figure 7A, B-B"), consistent with the fact that full-length kinesin motors are often autoinhibited (Verhey and Hammond, 2009; Brunnbauer et al., 2010). By contrast, a truncated version of Kif9 containing only the motor domain and a portion of the coiled-coiled domain bound strongly to microtubules (Figure 7A', 7C-C"). Moreover, live time-lapse imaging revealed processive movement of Kif9 along microtubules in a unidirectional manner (Movie 7, Figure 7D-D" arrow following Kif9 puncta). Kymographs confirmed processivity *in vitro*, albeit at relatively slow rates, 7.2 nm/second with an average of 790 nanometer run lengths and 122 second dwell times respectively (Figure 7E, Supp. Figure 3A-C).

As an active motor, Kif9 could function in the axoneme either as a traditional transport motor (i.e. analogous to an IFT kinesin) or in an active array (i.e. analogous to an axonemal dynein). To explore these possibilities, we expressed Kif9-GFP in motile axonemes, performed time-lapse imaging, and examined kymographs. In the vast majority of nearly 100 axonemes imaged, we observed negligible long-range movement of Kif9-GFP (Fig. 7F; Movie 8; Supp Figure 3B). In rare cases, however, we did observe faint traces indicating movement of Kif9-GFP (Supp. Figure 3C, arrows). Curiously, these traces indicated both anterograde and retrograde movement, with calculated transport rates of ~600 nanometers/sec, a rate similar to that of IFT transport in the axoneme (Wingfield et al., 2018; Craft et al., 2015; Brooks and Wallingford, 2012). Thus, we conclude that the vast majority of Kif9 in the axoneme is stationary and suggest that Kif9 may be transported in the axoneme by IFT.

### **Discussion:**

The normal and effective beating of 9+2 motile cilia on multiciliated cells, requires the action of the inner and outer dynein arms, the radial spokes, and the central pair, but how these systems work in concert remains poorly understood. Here, we extend previous studies of the central pair kinesin Klp1 in *Chlamydomonas* by showing that the vertebrate ortholog Kif9 is not only required for ciliary beating, but also has processive motor activity and is required for the organization of the distal axoneme in multiciliated cells. The work provides several new insights into the cell biology of ciliary beating.

First, the function of the central pair has been postulated to control beat and waveform through mechanical links to radial spoke and inner and outer dynein arms (Oda et al., 2014). Several studies have shown a physical link between central pair apparatus and radial spoke head proteins that occurs when cilia are undergoing "bending" during beat (Goodenough and Heuser, 1985; Oda et al., 2014; Warner, 1970). However, which proteins create this link is unknown. One hypothesis is that a microtubule motor protein, such as a kinesin motor, could serve this function as it could bind the central pair of microtubules and adjacent proteins and use its motor activity to fine tune beat and waveform through motor action, much like the action of axonemal dyneins (Viswanadha et al., 2017). Our data are consistent with this model.

We found that Kif9 is processive *in vitro*, but only very rarely showed any processive movement in MCC axonemes *in vivo*; the vast majority was restricted from long-range movement within the axonemes (97/100 kymographs examined). This result is exciting for its similarity to that of axonemal dyneins, which also display processivity *in vitro*, but are not processive *in vivo* and participate strictly in force generation effecting ciliary beating (Sakakibara et al., 1999). Indeed, a recent of the Cryo-EM structure of the active *Chlamydomonas* central apparatus further confirms that the Kif9 ortholog Klp1 forms active motor arrays on the C2 microtubule, suggesting a role in ciliary beating (Han et al., 2022). Our data therefore suggest that a similar mechanism of action is conserved in vertebrate motile cilia. Moreover, of the infrequent transport events observed of Kif9 *in vivo* (3/100 kymographs), two important notes are necessary to point out: (1) it is bidirectional in the axoneme, suggesting that Kif9 motor activity does not drive such movement; as an N-type kinesin Kif9 should only move towards plus ends, and (2) it is near the rate of IFT transport reported in axonemes previously (Wingfield et al., 2018; Craft et al., 2015; Brooks and Wallingford, 2012). This suggest that these few captured instances of Kif9 movement may actually be IFT transport of Kif9 into and out of the axoneme and not Kif9 movement along axonemes itself. On this note, it will be interesting then to directly test the possibility that Kif9 may be a cargo of the IFT system in vertebrate MCCs.

In motile axonemes also display a specific proximodistal patterning, and our data suggest a role, though likely indirect, for Kif9 in this patterning. Dynein arms, radial spoke, and central pair proteins decorate the majority of MCC motile cilia, but are excluded from a specific tip domain characterized by several cell-type specific “capping” structures (Soares et al., 2019; Dentler and Lecluyse, 1982; Portman et al., 1987; LeCluyse and Dentler, 1984). What proteins contribute to these structures remains unclear, but in *Xenopus*, Spef1 is enriched (Gray et al., 2009), Figure 5A). Spef1 is necessary for central pair formation in mouse testes and ependymal cell culture and functions *in vitro* as a microtubule bundling protein (Chan et al., 2005; Zheng et al., 2019, 1), and we show here that it is also enriched in the distal tip of mouse and human airway MCCs. Moreover, we now show that loss of Kif9 leads to loss of the Spef1 distal tip domain, though two other distal tip proteins, Eb1 and Eb3 remain unaffected (Figure 8B). Interestingly, several different central pair mutants in *Chlamydomonas* have shorter cilia (Lechtreck et al., 2013), and we speculate this decrease in length may arise from loss of distal tip integrity in these mutants. Additionally, although Kif9 knockdown beating defects in our system appear generally similar to that of the *Chlamydomonas* knockdown of Klp1 (Yokoyama et al., 2004), these phenotypes differ slightly from the more subtle phenotypes in mouse sperm flagella (Miyata et al., 2020). We conjecture that these differences may arise do to distinct tip structures and/or axoneal components the different ciliary subtypes (Soares et al., 2019).

Finally, the disruption of patterning of all major motility complexes in Kif9 knockdown cilia (Fig. 8), and the shorter overall length of these cilia lead us to speculate that IFT transport may be defective in Kif9 knockdown cilia. In *Chlamydomonas*, impairment of IFT has been observed in several central pair mutants (Lechtreck et al., 2013), and we can envision three different mechanisms by which IFT could be disrupted by loss of Kif9. In one scenario, a general derangement of the axoneme may impair normal IFT by simple structural means. Alternatively, defects in the distal tip could disrupt the normal re-organization of IFT particles as they shift from antero- to retrograde transport, resulting in disrupted IFT. Finally, loss of the distal tip could lead to shorter cilia in general through axonemal disassembly mechanisms and may also lead to derangement of IFT. Future experiments exploring these possibilities will be of interest.

In conclusion, we show here that vertebrate Kif9 is required for ciliary beating in MCCs, and for the normal localization of three major motility complexes in motile axonemes. Moreover, Kif9 is a processive motor *in vitro*, and consistent with data from *Chlamydomonas*, most likely acts to drive MT sliding in the central pair, thereby facilitating ciliary beat.

**Acknowledgements:** We thank members of the Wallingford and Gray Labs for critical comments and thoughtful feedback. This work was supported by grant funding: MJK supported by Provosts Graduate Excellence Fellowship, University of Texas at Austin. RSG supported by NIAMS R01AR072009. AH supported by K08HL150223. SB supported by HL128370. KJV supported by NIH R35GM131744. JBW supported by R01HL117164.

## **Methods and Materials:**

### ***Xenopus* embryo manipulations:**

*Xenopus* embryo manipulations were carried out using the standard protocols. Briefly, female adult *Xenopus* were induced to ovulate by injection of hCG (human chorionic gonadotropin). *In vitro* fertilization was carried out by homogenizing a small fraction of a testis in 1/3 X Marc's Modified Ringer's (MMR). Embryos were de-jellied in 1/3x MMR with 2.5-3% L-cysteine (pH 7.8-8). Embryos were microinjected with mRNA and morpholinos in 2% Ficoll (w/v) in 1/3x MMR. Embryos were washed with 1/3x MMR 1 hour post injection. Each injection was repeated 3-4 times across several days and clutches of embryos.

### **Microinjections:**

Gene sequences were obtained from Xenbase (<http://www.xenbase.org>). Open reading frames (ORF) of genes were amplified from the *Xenopus* cDNA library by polymerase chain reaction (PCR), and then inserted into a pCS vectors containing a fluorescence tag. The following constructs were cloned into pCS10R vector: GFP-dnai1, GFP-nme5 (Rsph23), RFP-clamp (spef1), GFP-spag16, GFP-Cfap74, GFP-Rsph10b, GFP-dnali1, eb3-GFP from (Shindo et al., 2008), eb1-GFP, membrane-RFP, membrane-GFP, membrane-BFP, Centrin4-RFP, and kif9-GFP. These constructs were linearized and capped mRNAs were synthesized using mMMESSAGE/mMACHINE SP6 transcription kit. Between 50-100pg of any given mRNA was injected into the two ventral blastomeres at the 4 cell stage. Kif9-GFP DNA was injected at 35pg. For rescue experiments 600pg of kif9 mRNA was injected. The kif9 morpholino was designed as a splice blocking morpholino to exon 1 of the kif9 mRNA sequence. The working concentration was 15ng and sequence as follows: 5' ATTCTCATATTCAATAGTCTTACCT 3'.

### **Imaging and Analysis:**

*Xenopus* embryos were grown up to stage 22-25 and mounted onto an imaging chamber in 1/3 MMR and live imaged immediately. The Bead flow movies and live cilia beat videos were taken on a Nikon W1 Spinning Disc Confocal at an image rate of 12.5 ms per frame. Live still images of axonemes were captured with a Zeiss LSM700 laser scanning confocal microscope with a 63x oil objective. Each experiment was repeated 3-4 times across several days and clutches of embryos. Approximately 15 different images (3-5 embryos) were taken for quantification, 5 different cilia per cell and at least three cells per image were quantified.

Beads (or microspheres) of size 1  $\mu$ m are added to the fluid medium for the purpose of tracing/visualizing and quantifying the fluid flow induced by the beating cilia. Bead flow movies were subjected to Flowtrace (Gilpin et al., 2017), for visualization of bead flow patterns across the epidermis. For this Flowtrace analysis, we selected an interrogation window size of 50 frames.

To quantify the fluid flow speeds, we carried out a Particle Image Velocimetry (PIV) analysis using the Matlab-based PIVlab package (Thielicke and Stamhuis, 2014). First, we extracted individual frames from the time-lapse datasets (movies) and we carried out the image preprocessing step by selecting the contrast limited adaptive histogram equalization (CLAHE) option (window size 20 px). Next, we proceeded with the PIV analysis using these settings: FFT window deformation, Interrogation area 128 x 128 pixels with 50% overlap (Pass 1), and with

interrogation area of 64 x 64 pixels with 50% overlap (Pass 2). After this step, the vector validation was done by choosing suitable velocity limits, standard deviation filters and interpolation of missing data. We carefully selected a rectangular region just adjacent and parallel to the ciliary beating surface on the embryo. We quantified the average speed in this selected region over time, and the error bars represent the standard deviation. This procedure was utilized for each individual dataset for the control, Kif9 and rescue cases. To obtain a characteristic speed for each case (control, Kif9 and rescue), further averaging was carried out: for control and Kif9 (N = 5 datasets), and for rescue (N = 10 datasets).

Quantification of cilia length, length of each construct along axonemes, and fluorescence intensity profiles were all taken in FIJI. Kymographs of cilia beat were also generated using FIJI. Briefly, lines were drawn, taking length measurements and fluorescence intensity profiles. Outputs were placed into GraphPad Prism 8 and graphs were generated. All statistical analyses were done in GraphPad Prism 8 with either t-tests or one-way Anovas where appropriately comparing three different groups of data.

### ***Xenopus* immunostaining:**

For immunostaining, protocols previously described in (Brooks and Wallingford, 2015) were followed. Briefly, wildtype and MO injected embryos were fixed with 4% PFA at stages 22-25 for 1 hour at RT. They were then washed with PBS + 0.1% Tween (PBST), and subsequently washed in MeOH. They were dehydrated and permeabilized in 100% MeOH at -20 degrees C for 30 minutes to 1 hour. Embryos were then rehydrated and washed with PBST. Embryos were then blocked for 1 hr at RT in 10% NGS, 5% DMSO in 1x PBST. Primary antibodies were incubated overnight and embryos were washed 3x in PBST, then incubated with secondary antibody for 1 hour at RT. A rabbit Kif9 antibody was used at 1:100 dilution from Atlas Antibodies (HPA022033). Mouse acetylated tubulin antibody was incubated at 1:1000 from Sigma (6-11B-1). Secondaries Alexa fluorophores anti-rabbit 488 and anti-mouse 647 were used at 1:1000 dilutions.

### **RT-PCR**

To verify the efficiency of our *Kif9* Morpholino, MO was injected into all 4 cells at the 4 cell stage and total RNA was isolated using the TRIreagent (Thermofischer) at stage 23. One microgram of mRNA was used to synthesize cDNA using iScript (Biorad). Kif9 and B-actin cDNAs were amplified by GoTag Green Master Mix (Promega) and with the following primers:

Bactin F1: 5' GCCCGCATAGAAAGGAGACAG 3'

Bactin F2: 5' CCAAACCTCGCTCAGTGACC 3'

Bactin R1: 5' TCATCCCAGTTGGTGACAATGC 3'

Bactin R2: 5' TCCATTCCAACCATGACACC 3'

Kif9 F1: 5' GAGACGGGATAGTTTACACACAGC 3'

Kif9 R1: 5' TGGAGGCAAGGTTTAGGGATAAGC 3'

Kif9 F2: 5' CGCTGAAGCCAAGAGCTGAAC 3'

Kif9 R2: 5' GCATCTGGAACAGTGGAAGGAG 3'

### **Airway epithelial cell culture and immunostaining:**

Human airway tracheas were retrieved from surgical excess of tracheobronchial segments of lungs donated for transplantation. Human tracheobronchial epithelial cells (hTEC) were isolated from sections of normal human trachea obtained from non-smoking donors lacking respiratory pathology. These unidentified tissues are exempt from regulation by HHS regulation 45 CFR Part 46. hTEC cells were expanded in-vitro and allowed to differentiate into ciliated cells using air-liquid interface (ALI) conditions on supported membranes (Transwell, Corning Inc., Corning, NY), as previously described (PMID: 12388377). Paraffin embedded tracheal sections or

cultured primary airway cells were fixed and immunostained as previously described (PMID: 17488776). Nuclei were stained using 4', 6-diamidino-2-phenylindole (DAPI, Vector Laboratories, Burlingame, CA, USA). KIF9, was detected using primary antibodies obtained from MilliporeSigma (St. Louis, MO, HPA022033). Basal bodies were detected using antibodies against Centrin (clone 20H5, MilliporeSigma). DNAI1, a marker of outer dynein arm, was detected using NeuroMab (UC Davis, Ca, clone UNC 65.56.18.11). Images were acquired using an epifluorescent microscope interfaced with imaging software (LAS X; Leica) and adjusted globally for brightness and contrast using Affinity Photo (Serif Ltd, Nottinghamshire, United Kingdom).

## **Single Molecule Microtubule Assays:**

### **Plasmid**

To generate pMT-*x*KIF9(1-461)-mNeonGreen plasmid, the coiled-coil prediction of full-length *x*KIF9 was carried out in Marcoil (Delorenzi and Speed, 2002) and COILS (Lupas, 1996). *x*KIF9(-461) truncation which includes the first two coiled coil domains and is expected to form a dimer was amplified by PCR from full-length *x*KIF9 and subcloned into pMT-mNeonGreen vector by NEBuilder HiFi DNA assembly cloning kit. The plasmid was verified by DNA sequencing.

### **Cell culture, transfection and lysate preparation**

*Drosophila* S2 cells were cultured in Schneider's *Drosophila* medium (Gibco) supplemented with 10% (vol/vol) FBS (HyClone) at 26°C. Plasmid for expression of *x*KIF9(1-461)-mNeonGreen in the pMT vector was transfected into S2 cells using Lipofectamine LTX Reagent with PLUS Reagent (Invitrogen) according to manufacturer's instructions. Expression of *x*KIF9(1-461)-mNeonGreen was induced by adding 1mM CuSO<sub>4</sub> to the medium after 4-5h transfection.

To prepare cell lysate for single molecule assays, S2 cells were harvested after 48h transfection. The cells were centrifuged at low speed at 4°C. The cell pellet was washed with PBS buffer and resuspended in ice-cold lysis buffer (25 mM HEPES/KOH, 115 mM potassium acetate, 5 mM sodium acetate, 5 mM MgCl<sub>2</sub>, 0.5 mM EGTA, and 1% Triton X-100, pH 7.4) freshly supplemented with 1 mM ATP, 1 mM PMSF, 1 mM DTT and protease inhibitors (Sigma-Aldrich). After the cell lysate was clarified by centrifugation at full-speed at 4°C, aliquots of the supernatant were snap frozen in liquid nitrogen and stored at -80°C until further use.

### **Single-molecule motility assays**

HiLyte647-labeled microtubules were polymerized from purified tubulin including 10% HiLyte647-labeled tubulin (Cytoskeleton) in BRB80 buffer (80 mM Pipes/KOH pH 6.8, 1 mM MgCl<sub>2</sub>, and 1 mM EGTA) supplemented with 1 mM GTP and 2.5 mM MgCl<sub>2</sub> at 37°C for 30 min. 20 μM taxol in prewarmed BRB80 buffer was added and incubated at 37°C for additional 30 min to stabilize microtubules. Microtubules were stored in the dark at room temperature for further use. A flow cell (~10 μl volume) was assembled by attaching a clean #1.5 coverslip (Fisher Scientific) to a glass slide (Fisher Scientific) with two strips of double-sided tape. Polymerized microtubules were diluted in BRB80 buffer supplemented with 10 μM taxol and then were infused into flow cells and incubated for 5 min at room temperature for nonspecific adsorption to the coverslips. Subsequently, blocking buffer (15 mg/ml BSA and 10 μM taxol in P12 buffer) was infused and incubated for 5min. Finally, kinesin motors in the motility mixture [2 mM ATP, 0.4 mg/ml casein, 6 mg/ml BSA, 10 μM taxol, and oxygen scavenging (1 mM DTT, 1 mM MgCl<sub>2</sub>, 10

mM glucose, 0.2 mg/ml glucose oxidase, and 0.08 mg/ml catalase) in P12 buffer] was added to the flow cells. The flow-cell was sealed with molten paraffin wax.

Images for single molecule assay were acquired by TIRF microscopy using an inverted microscope Ti-E/B (Nikon) equipped with the perfect focus system (Nikon), a 100× 1.49 NA oil immersion TIRF objective (Nikon), three 20-mW diode lasers (488 nm, 561 nm, and 640 nm) and an electron-multiplying charge-coupled device detector (iXon X3DU897; Andor Technology). Image acquisition was controlled using Nikon Elements software and all assays were performed at room temperature. Images were acquired continuously every 5 s for 5 min. Maximum-intensity projections were generated and the kymographs were produced by drawing along tracks of motors (width= 3 pixels) using Fiji/ImageJ2.

## References

- Bernstein, M., P.L. Beech, S.G. Katz, and J.L. Rosenbaum. 1994. A new kinesin-like protein (Klp1) localized to a single microtubule of the *Chlamydomonas* flagellum. *J Cell Biol.* 125:1313–1326. doi:10.1083/jcb.125.6.1313.
- Brooks, E.R., and J.B. Wallingford. 2012. Control of vertebrate intraflagellar transport by the planar cell polarity effector Fuz. *J Cell Biol.* 198:37–45. doi:10.1083/jcb.201204072.
- Brooks, E.R., and J.B. Wallingford. 2014. Multiciliated Cells. *Current Biology.* 24:R973–R982. doi:10.1016/j.cub.2014.08.047.
- Brooks, E.R., and J.B. Wallingford. 2015. Chapter 7 - In vivo investigation of cilia structure and function using *Xenopus*. *In Methods in Cell Biology.* R. Basto and W.F. Marshall, editors. Academic Press. 131–159.
- Brunnbauer, M., F. Mueller-Planitz, S. Kösem, T.H. Ho, R. Dombi, J.C.M. Gebhardt, M. Rief, and Z. Ökten. 2010. Regulation of a heterodimeric kinesin-2 through an unprocessive motor domain that is turned processive by its partner. *PNAS.* 107:10460–10465. doi:10.1073/pnas.1005177107.
- Bui, K.H., T. Yagi, R. Yamamoto, R. Kamiya, and T. Ishikawa. 2012. Polarity and asymmetry in the arrangement of dynein and related structures in the *Chlamydomonas* axoneme. *Journal of Cell Biology.* 198:913–925. doi:10.1083/jcb.201201120.
- Chan, S.W., K.J. Fowler, K.H.A. Choo, and P. Kalitsis. 2005. Spef1, a conserved novel testis protein found in mouse sperm flagella. *Gene.* 353:189–199. doi:10.1016/j.gene.2005.04.025.
- Cho, E.H., H.J. Huh, I. Jeong, N.Y. Lee, W.-J. Koh, H.-C. Park, and C.-S. Ki. 2020. A nonsense variant in NME5 causes human primary ciliary dyskinesia with radial spoke defects. *Clinical Genetics.* 98:64–68. doi:10.1111/cge.13742.
- Craft, J.M., J.A. Harris, S. Hyman, P. Kner, and K.F. Lehtreck. 2015. Tubulin transport by IFT is upregulated during ciliary growth by a cilium-autonomous mechanism. *Journal of Cell Biology.* 208:223–237. doi:10.1083/jcb.201409036.
- Dai, D., M. Ichikawa, K. Peri, R. Rebinsky, and K.H. Bui. 2020. Identification and mapping of central pair proteins by proteomic analysis. *Biophysics and Physicobiology.* 17:71–85. doi:10.2142/biophysico.BSJ-2019048.

- Dentler, W.L., and E.L. Lecluyse. 1982. Microtubule capping structures at the tips of tracheal cilia: Evidence for their firm attachment during ciliary bend formation and the restriction of microtubule sliding. *Cell Motility*. 2:549–572. doi:10.1002/cm.970020605.
- Fliegau, M., H. Olbrich, J. Horvath, J.H. Wildhaber, M.A. Zariwala, M. Kennedy, M.R. Knowles, and H. Omran. 2005. Mislocalization of DNAH5 and DNAH9 in Respiratory Cells from Patients with Primary Ciliary Dyskinesia. *Am J Respir Crit Care Med*. 171:1343–1349. doi:10.1164/rccm.200411-1583OC.
- Gilpin, W., V.N. Prakash, and M. Prakash. 2017. Flowtrace: simple visualization of coherent structures in biological fluid flows. *Journal of Experimental Biology*. 220:3411–3418. doi:10.1242/jeb.162511.
- Goodenough, U.W., and J.E. Heuser. 1985. Substructure of inner dynein arms, radial spokes, and the central pair/projection complex of cilia and flagella. *Journal of Cell Biology*. 100:2008–2018. doi:10.1083/jcb.100.6.2008.
- Gray, R.S., P.B. Abitua, B.J. Wlodarczyk, H.L. Szabo-Rogers, O. Blanchard, I. Lee, G.S. Weiss, K.J. Liu, E.M. Marcotte, J.B. Wallingford, and R.H. Finnell. 2009. The planar cell polarity effector Fuz is essential for targeted membrane trafficking, ciliogenesis and mouse embryonic development. *Nat Cell Biol*. 11:1225–1232. doi:10.1038/ncb1966.
- Han, L., Q. Rao, R. Yang, Y. Wang, P. Chai, Y. Xiong, and K. Zhang. 2022. Cryo-EM structure of an active central apparatus.
- Ishikawa, T. 2017. Axoneme Structure from Motile Cilia. *Cold Spring Harb Perspect Biol*. 9:a028076. doi:10.1101/cshperspect.a028076.
- Konjikusic, M.J., R.S. Gray, and J.B. Wallingford. 2021. The developmental biology of kinesins. *Developmental Biology*. 469:26–36. doi:10.1016/j.ydbio.2020.09.009.
- Lechtreck, K.-F., T.J. Gould, and G.B. Witman. 2013. Flagellar central pair assembly in *Chlamydomonas reinhardtii*. *Cilia*. 2:15. doi:10.1186/2046-2530-2-15.
- Lechtreck, K.-F., and G.B. Witman. 2007. *Chlamydomonas reinhardtii* hidin is a central pair protein required for flagellar motility. *Journal of Cell Biology*. 176:473–482. doi:10.1083/jcb.200611115.
- LeCluyse, E.L., and W.L. Dentler. 1984. Asymmetrical microtubule capping structures in frog palate cilia. *Journal of Ultrastructure Research*. 86:75–85. doi:10.1016/S0022-5320(84)90097-2.
- Loges, N.T., H. Olbrich, L. Fenske, H. Mussaffi, J. Horvath, M. Fliegau, H. Kuhl, G. Baktai, E. Peterffy, R. Chodhari, E.M.K. Chung, A. Rutman, C. O’Callaghan, H. Blau, L. Tiszlavicz, K. Voelkel, M. Witt, E. Zietkiewicz, J. Neesen, R. Reinhardt, H.M. Mitchison, and H. Omran. 2008. DNAI2 mutations cause primary ciliary dyskinesia with defects in the outer dynein arm. *Am J Hum Genet*. 83:547–558. doi:10.1016/j.ajhg.2008.10.001.
- Loreng, T.D., and E.F. Smith. 2017. The Central Apparatus of Cilia and Eukaryotic Flagella. *Cold Spring Harb Perspect Biol*. 9:a028118. doi:10.1101/cshperspect.a028118.

- Louka, P., K.K. Vasudevan, M. Guha, E. Joachimiak, D. Wloga, R.F.-X. Tomasi, C.N. Baroud, P. Dupuis-Williams, D.F. Galati, C.G. Pearson, L.M. Rice, J.J. Moresco, J.R. Yates III, Y.-Y. Jiang, K. Lehtreck, W. Dentler, and J. Gaertig. 2018. Proteins that control the geometry of microtubules at the ends of cilia. *Journal of Cell Biology*. 217:4298–4313. doi:10.1083/jcb.201804141.
- Miyata, H., K. Shimada, A. Morohoshi, S. Oura, T. Matsumura, Z. Xu, Y. Oyama, and M. Ikawa. 2020. Testis-enriched kinesin KIF9 is important for progressive motility in mouse spermatozoa. *The FASEB Journal*. 34:5389–5400. doi:10.1096/fj.201902755R.
- Oda, T., H. Yanagisawa, T. Yagi, and M. Kikkawa. 2014. Mechanosignaling between central apparatus and radial spokes controls axonemal dynein activity. *Journal of Cell Biology*. 204:807–819. doi:10.1083/jcb.201312014.
- Pedersen, L.B., S. Geimer, R.D. Sloboda, and J.L. Rosenbaum. 2003. The Microtubule Plus End-Tracking Protein EB1 Is Localized to the Flagellar Tip and Basal Bodies in *Chlamydomonas reinhardtii*. *Current Biology*. 13:1969–1974. doi:10.1016/j.cub.2003.10.058.
- Portman, R.W., E.L. LeCluyse, and W.L. Dentler. 1987. Development of microtubule capping structures in ciliated epithelial cells. *J Cell Sci*. 87 ( Pt 1):85–94.
- Sakakibara, H., H. Kojima, Y. Sakai, E. Katayama, and K. Oiwa. 1999. Inner-arm dynein c of *Chlamydomonas* flagella is a single-headed processive motor. *Nature*. 400:586–590. doi:10.1038/23066.
- Schrøder, J.M., J. Larsen, Y. Komarova, A. Akhmanova, R.I. Thorsteinsson, I. Grigoriev, R. Manguso, S.T. Christensen, S.F. Pedersen, S. Geimer, and L.B. Pedersen. 2011. EB1 and EB3 promote cilia biogenesis by several centrosome-related mechanisms. *J Cell Sci*. 124:2539–2551. doi:10.1242/jcs.085852.
- Sha, Y., X. Wei, L. Ding, Z. Ji, L. Mei, X. Huang, Z. Su, W. Wang, X. Zhang, and S. Lin. 2020. Biallelic mutations of CFAP74 may cause human primary ciliary dyskinesia and MMAF phenotype. *J Hum Genet*. 65:961–969. doi:10.1038/s10038-020-0790-2.
- Shindo, A., T.S. Yamamoto, and N. Ueno. 2008. Coordination of Cell Polarity during *Xenopus* Gastrulation. *PLOS ONE*. 3:e1600. doi:10.1371/journal.pone.0001600.
- Soares, H., B. Carmona, S. Nolasco, L. Viseu Melo, and J. Gonçalves. 2019. Cilia Distal Domain: Diversity in Evolutionarily Conserved Structures. *Cells*. 8:160. doi:10.3390/cells8020160.
- Spassky, N., and A. Meunier. 2017. The development and functions of multiciliated epithelia. *Nat Rev Mol Cell Biol*. 18:423–436. doi:10.1038/nrm.2017.21.
- Thielicke, W., and E. Stamhuis. 2014. PIVlab – Towards User-friendly, Affordable and Accurate Digital Particle Image Velocimetry in MATLAB. *Journal of Open Research Software*. 2:e30. doi:10.5334/jors.bl.
- Verhey, K.J., and J.W. Hammond. 2009. Traffic control: regulation of kinesin motors. *Nature Reviews Molecular Cell Biology*. 10:765–777. doi:10.1038/nrm2782.

- Viswanadha, R., W.S. Sale, and M.E. Porter. 2017. Ciliary Motility: Regulation of Axonemal Dynein Motors. *Cold Spring Harb Perspect Biol.* 9:a018325. doi:10.1101/cshperspect.a018325.
- Walentek, P., and I.K. Quigley. 2017. What we can learn from a tadpole about ciliopathies and airway diseases: Using systems biology in *Xenopus* to study cilia and mucociliary epithelia. *genesis.* 55:e23001. doi:10.1002/dvg.23001.
- Warner, F.D. 1970. NEW OBSERVATIONS ON FLAGELLAR FINE STRUCTURE : The Relationship Between Matrix Structure and the Microtubule Component of the Axoneme. *Journal of Cell Biology.* 47:159–182. doi:10.1083/jcb.47.1.159.
- Wingfield, J.L., K.-F. Lechtreck, and E. Lorentzen. 2018. Trafficking of ciliary membrane proteins by the intraflagellar transport/BBSome machinery. *Essays in Biochemistry.* 62:753–763. doi:10.1042/EBC20180030.
- Yamamoto, R., M. Hirono, and R. Kamiya. 2010. Discrete PIH proteins function in the cytoplasmic preassembly of different subsets of axonemal dyneins. *Journal of Cell Biology.* 190:65–71. doi:10.1083/jcb.201002081.
- Yokoyama, R., E. O'Toole, S. Ghosh, and D.R. Mitchell. 2004. Regulation of flagellar dynein activity by a central pair kinesin. *PNAS.* 101:17398–17403. doi:10.1073/pnas.0406817101.
- Zhao, L., Y. Hou, T. Picariello, B. Craige, and G.B. Witman. 2019. Proteome of the central apparatus of a ciliary axoneme. *J Cell Biol.* 218:2051–2070. doi:10.1083/jcb.201902017.
- Zheng, J., H. Liu, L. Zhu, Y. Chen, H. Zhao, W. Zhang, F. Li, L. Xie, X. Yan, and X. Zhu. 2019. Microtubule-bundling protein Spf1 enables mammalian ciliary central apparatus formation. *J Mol Cell Biol.* 11:67–77. doi:10.1093/jmcb/mjy014.
- Zheng, W., F. Li, Z. Ding, H. Liu, L. Zhu, C. Xu, J. Li, Q. Gao, Y. Wang, Z. Fu, C. Peng, X. Yan, X. Zhu, and Y. Cong. 2021. Distinct architecture and composition of mouse axonemal radial spoke head revealed by cryo-EM. *PNAS.* 118. doi:10.1073/pnas.2021180118.

## Figures

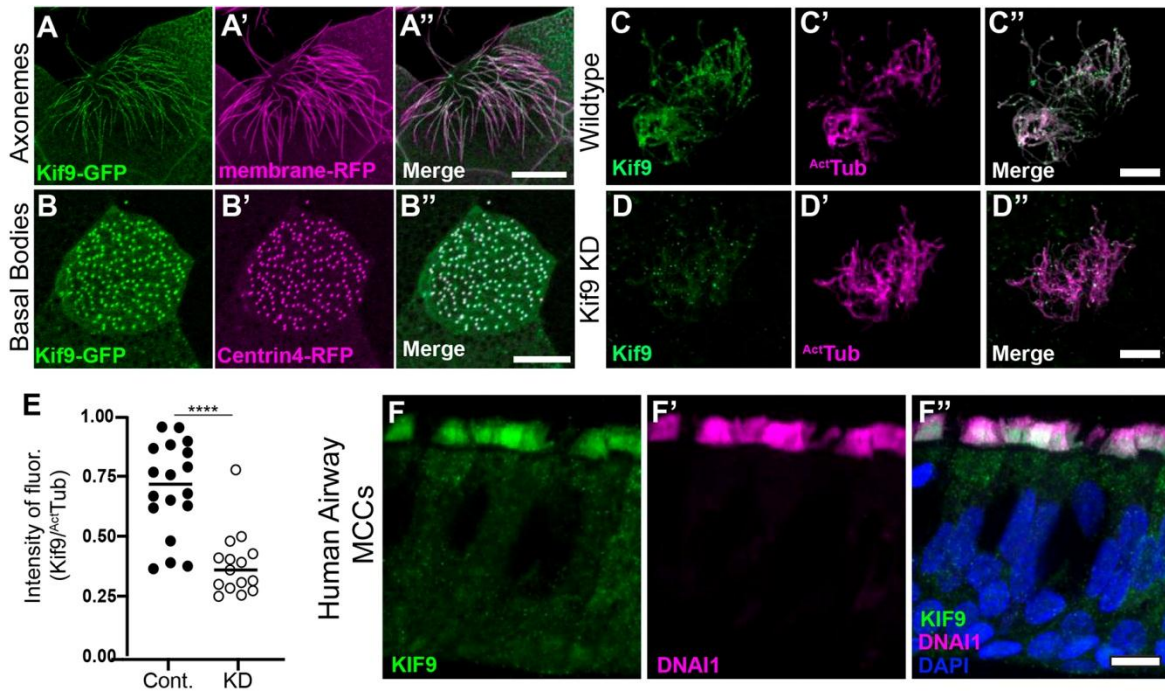


**Figure 1. Kif9 localization to motile cilia.** A-A''. Kif9-GFP construct localizes to xenopus multiciliated cells in the axonemes. Kif9-GFP in green (A), membrane-RFP in magenta (A'). B-B''. Kif9-GFP construct localizes to basal bodies of multiciliated cells in *Xenopus*. Kif9-GFP in Green (B), Centrin4-RFP in magenta (B'). Scale bars for A-B'' 10uM. C-C''. Kif9 antibody (green) confirms localization to xenopus axonemes. Kif9 in green (C) and acetylated tubulin in magenta (C') Scale bars 10uM. D-D''. Knockdown with 15 ng of morpholino reduces Kif9 (green) from cilium. E. Quantification of Kif9 staining intensity over the intensity of acetylated tubulin in control and morpholino injected frogs. F-F''. KIF9 immunostaining in human airway multiciliated cells. F. KIF9 immunostaining (green). F' DNAI1 immunostaining (magenta). F'' Merge of F-F' with DAPI. Scale Bar 10 microns.

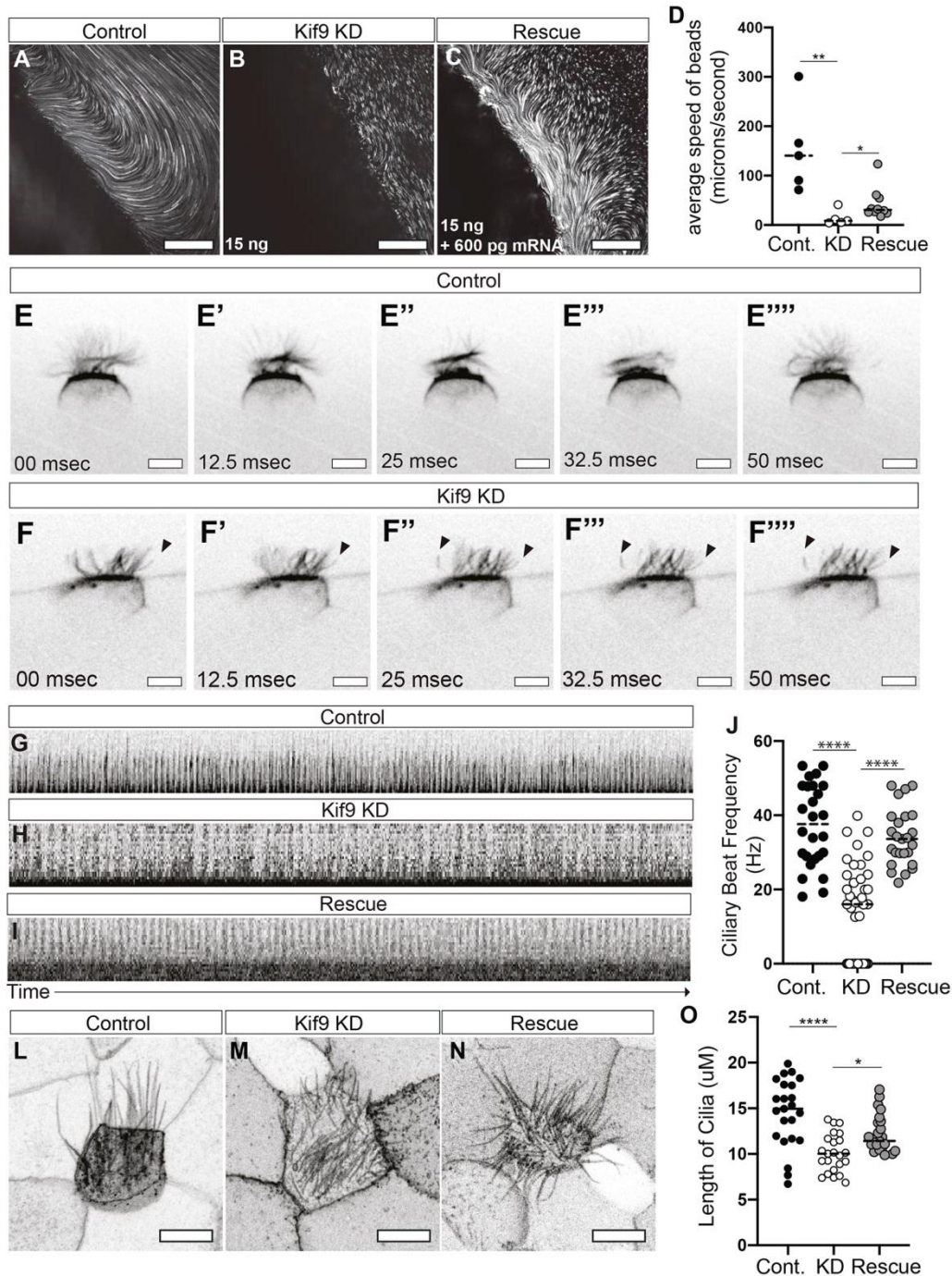


**Figure 2. Kif9 is necessary for ciliary beating and ciliary length.** **A-C.** Still images from bead flow movies subjected to Flowtrace analysis. (A) Control injected, (B) 15 ng Kif9 morpholino injected, and (C) 15ng morpholino with 600pg Kif9 mRNA (Rescue) Note: Movie 3 shows a different flow plane than 1 and 2 hence the different direction of flow in Movie 3, but was most representative of average flow rescues). Scale bars for A-C 50 microns. **D.** Graph of bead beat velocity averages from collected movies. P-values: \*\* = 0.0094 and \* = 0.0280. **E-F'''.** Still frames of ciliary beating in control (E-E''') and Kif9 KD (F-F''') multiciliated cells. Arrowheads point to stalled/paralyzed cilia frequently observed in Kif9 KD embryos. Scale bar is 10 microns. **G-I.** Representative kymographs of ciliary beating in Control (G), Kif9 KD (H), and Rescue (I)

injected embryos. J. Graph of ciliary beat frequency calculated from kymographs of 27 different movies of cilia beating in Hertz. L-N. Representative images of ciliary length marked with membrane-GFP in Control (L), Kif9 morpholino (M), and Rescue (N) injected embryos. Note: The variability in cilia numbers in these images reflect the normally high variability seen in *Xenopus* MCCs. Scale bars 10 microns. O. Graph of ciliary length from Control, Morpholino, or Rescue in microns. P-values: \*\*\*\* < 0.0001 and \* = 0.0174.

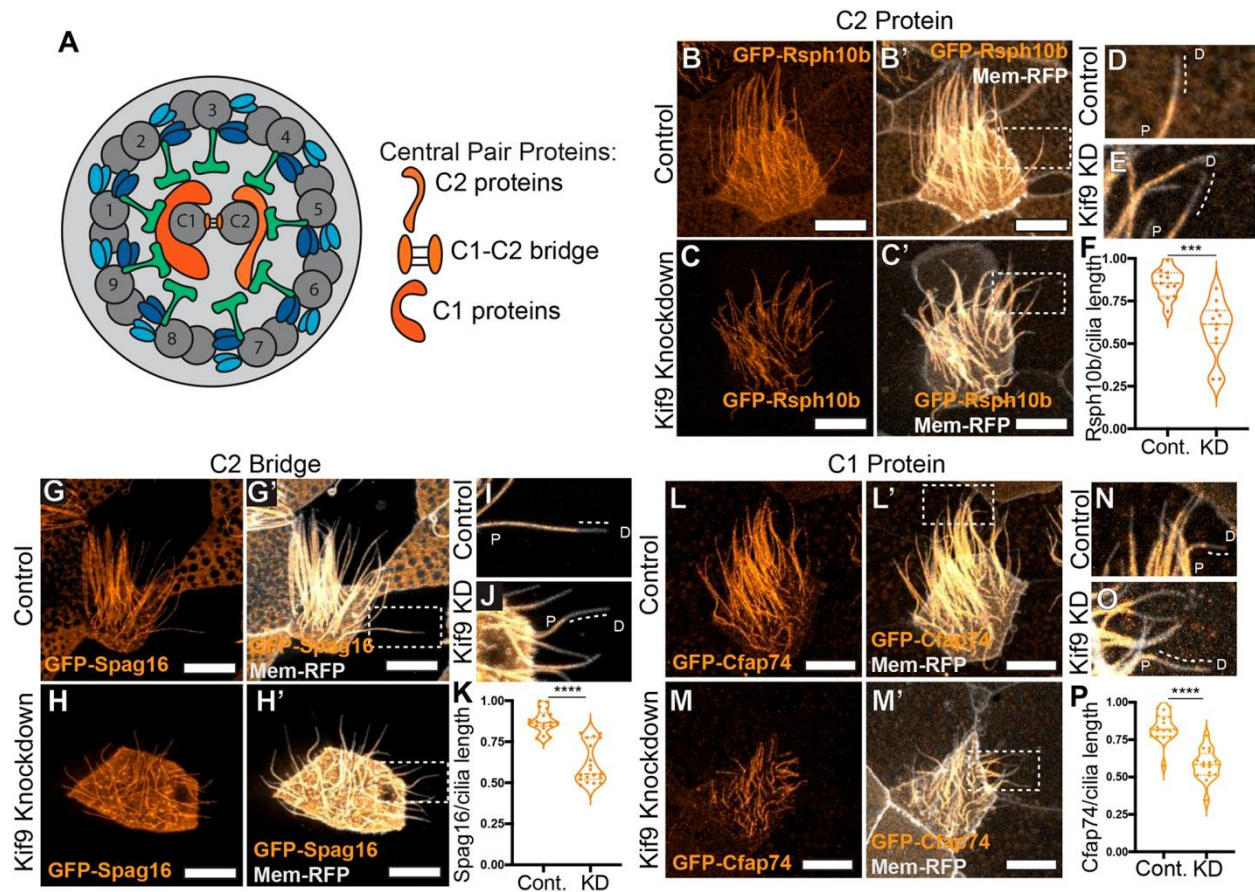


**Figure 3. Kif9 contributes to central pair proteins and distal tip compartmentalization.** A. Schematic of 9+2 motile cilium structure with central pair components schematized by tubule association. B-C'. Confocal images of radial spoke head component GFP-Rsph10B (orange) localization in Control (B-B') and Kif9 Morpholino (C-C') injected embryos. D-E. Magnified insets of cilia in Control (D) and (E) Kif9 knockdown cilia showing loss of GFP-Rsph10B (orange) from the distal ends of cilia. Dotted line outlining lack of protein at distal ends. P = Proximal, D = Distal. F. Quantification of GFP-Rsph10B length over total ciliary length in Control and Kif9 knockdown embryos. G-H'. Confocal images of GFP-Spag16 (orange) and membrane-RFP (grays) localization in *Xenopus* Multiciliated cells in Control (G-G'), Kif9 Morpholino (H-H') injected embryos. I-J. Magnified insets of distal tips of cilia in Control (I) and Kif9 Knockdown (J) cilia showing loss of GFP-Spag16 (orange) from the distal tip of cilia. Dotted line outlining lack of protein at distal ends. P = Proximal, D = Distal. K. Quantification of GFP-Spag16 length over total ciliary length in Control and Kif9 Knockdown injected embryos. P-value = \*\*\*\* < 0.0001. L-M'. Confocal images of GFP-Cfap74 localization in Control (L-L') and Kif9 Morpholino (M-M') injected embryos. N-O. Magnified insets of distal tips of cilia in Control (N) and Kif9 knockdown (O) cilia showing loss of GFP-Cfap74 (orange) from the distal tip of cilia. Dotted line outlining lack of protein at distal ends. P = Proximal, D = Distal. P. Quantification of GFP-Cfap74 length over total ciliary length in Control and Kif9 knockdown embryos. All scale bars 10  $\mu$ m.

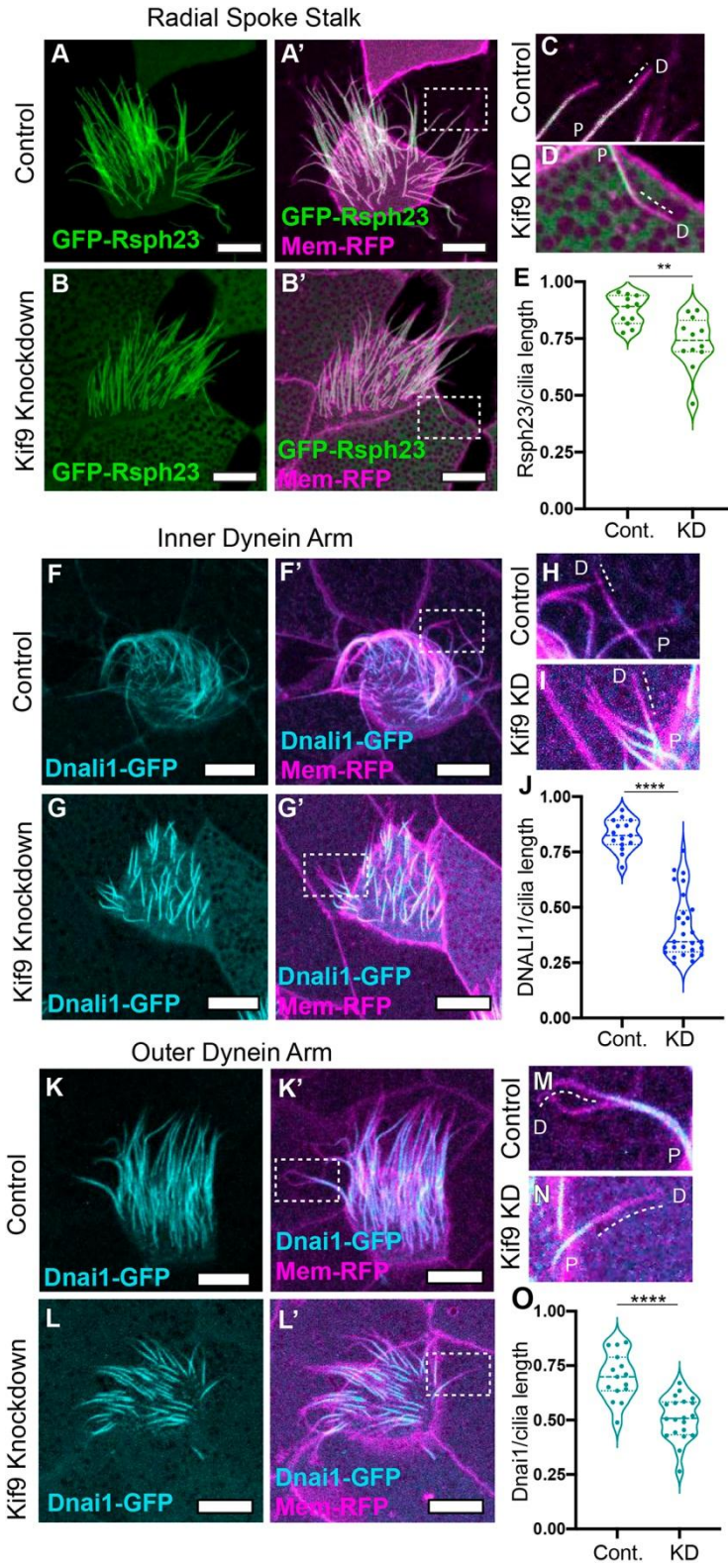


**Figure 4. Kif9 is necessary for Radial Spoke, Inner Dynein Arm and Outer Dynein Arm placement in the distal ends of cilia.**

A-B'. Confocal images of radial spoke stalk component GFP-Rsph23 (green) localization in Control (A-A') and Kif9 Morpholino (B-B') injected embryos. C-D. Magnified insets of cilia in Control (C) and Kif9 knockdown (D) cilia showing loss of GFP-Rsph23 from the distal ends of cilia. Dotted line outlining lack of protein at distal ends. P = Proximal, D = Distal. E. Quantification of GFP-Rsph23 length over total ciliary length in Control and Kif9 knockdown embryos. F-G'. Confocal images of inner dynein arm Dnali1-GFP localization in Control (F-F') and Kif9 Morpholino (G-G') injected embryos. H-I. Magnified insets of cilia in Control (H) and Kif9 knockdown (I) cilia showing loss of Dnali1-GFP from the distal ends of cilia. Dotted line outlining lack of protein at distal ends. P = Proximal, D = Distal. J. Quantification of GFP-Dnai1 length over total ciliary length in Control and Kif9 knockdown embryos. K-L'. Confocal images of outer dynein arm GFP-Dnai1 (cyan) localization in Control (K-K') and Kif9 Morpholino (L-L') injected embryos. M-N. Magnified insets of cilia in Control (M) and Kif9 knockdown (N) cilia showing loss of GFP-Dnai1 (cyan) from the distal ends of cilia. Dotted line outlining lack of protein at distal ends. P = Proximal, D = Distal. O. Quantification of GFP-Dnai1 length over total ciliary length in Control and Kif9 knockdown embryos. All scale bars 10uM.

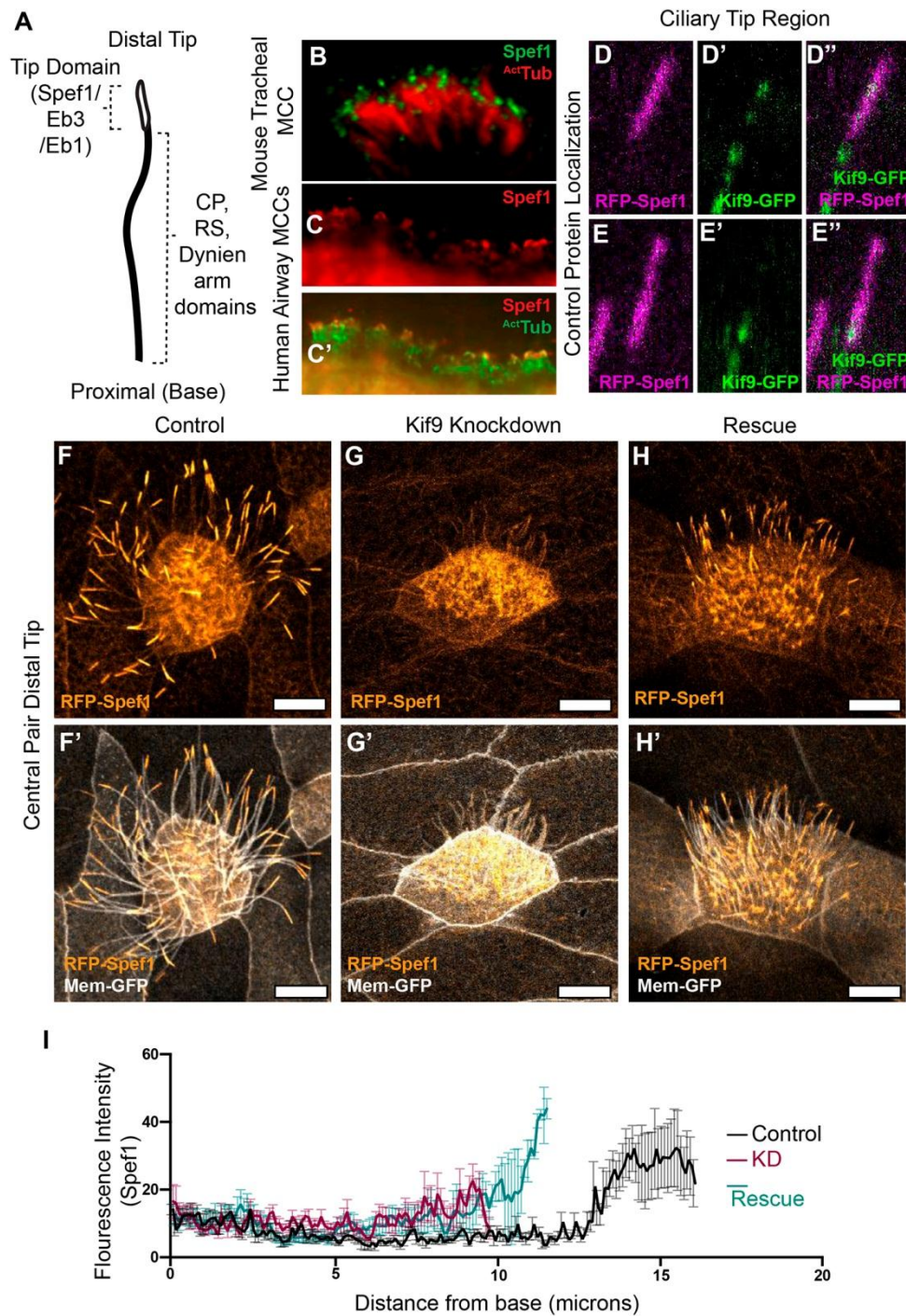


**Figure 5. Kif9 contributes to distal tip integrity.** A. Schematic of proximal to distal patterning of the motile cilium. Tip domain schematized with proteins known to localize to that domain, as well as proteins localizing to the rest of the axonemes. B. Images of immunostaining of Spef1 in mouse tracheal multiciliated cells. Spef1 in green, Acetylated Tubulin in red. C-D. Images of immunostaining of human airway multiciliated cells. Spef1 in red, Acetylated Tubulin in green. D-E". Confocal Images of RFP-Spef1 (magenta) and Kif9-GFP (green) colocalization in the

distal tips of the cilium. F-H'. Confocal images of RFP-Spef1 (orange) and Membrane-GFP (grays) in Control (F-F'), Kif9 morpholino injected (G-G'), and Rescue (H-H') embryos. I. Graph of fluorescence intensity line traces of RFP-Spef1 in Control, Knockdown, and Rescue cilia. All scale bars 10 microns.

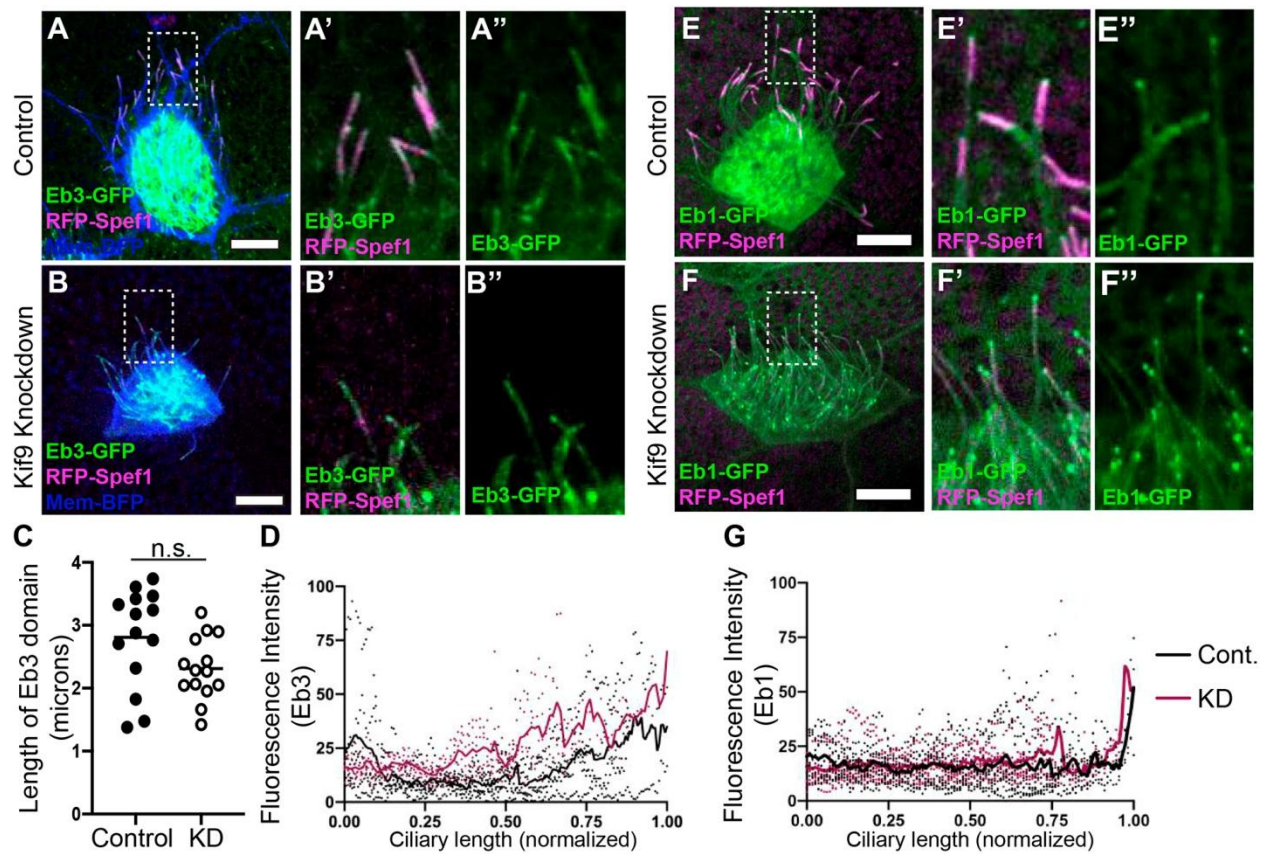


**Figure 6. Microtubule plus-end binding proteins Eb1 and Eb3 remain unaffected in the distal tip by knockdown of Kif9.** A-B". Confocal images of Control (A-A") and Kif9 morpholino injected embryos (B-B") with Eb3-GFP (green), RFP-Spef1 (magenta), and Membrane-BFP (blue). A'-B'. Insets of ciliary tips with Eb3-GFP (green) and RFP-Spef1 (magenta) in Control and Knockdown cilia. A"-B". Insets with Eb3 alone in Control and Knockdown cilia. C. Length measurements of Eb3 domain in Control and Kif9 knockdown embryos. P-value = 0.056. D. Graph of line traces of fluorescence intensities of Eb3 in Control and Knockdown cilia. E-F". Confocal images of Control (E-E") and Kif9 morpholino injected embryos (F-F") with Eb1-GFP (green), RFP-Spef1 (magenta), and Membrane-BFP (blue). E'-F'. Insets of ciliary tips with Eb1-GFP (green) and RFP-Spef1 (magenta) in Control and Knockdown cilia. E"-F". Insets of Eb1 alone in Control and Knockdown cilia. G. Graph of line traces of fluorescence intensities of Eb1 in Control and Knockdown cilia. All scale bars 10 microns.

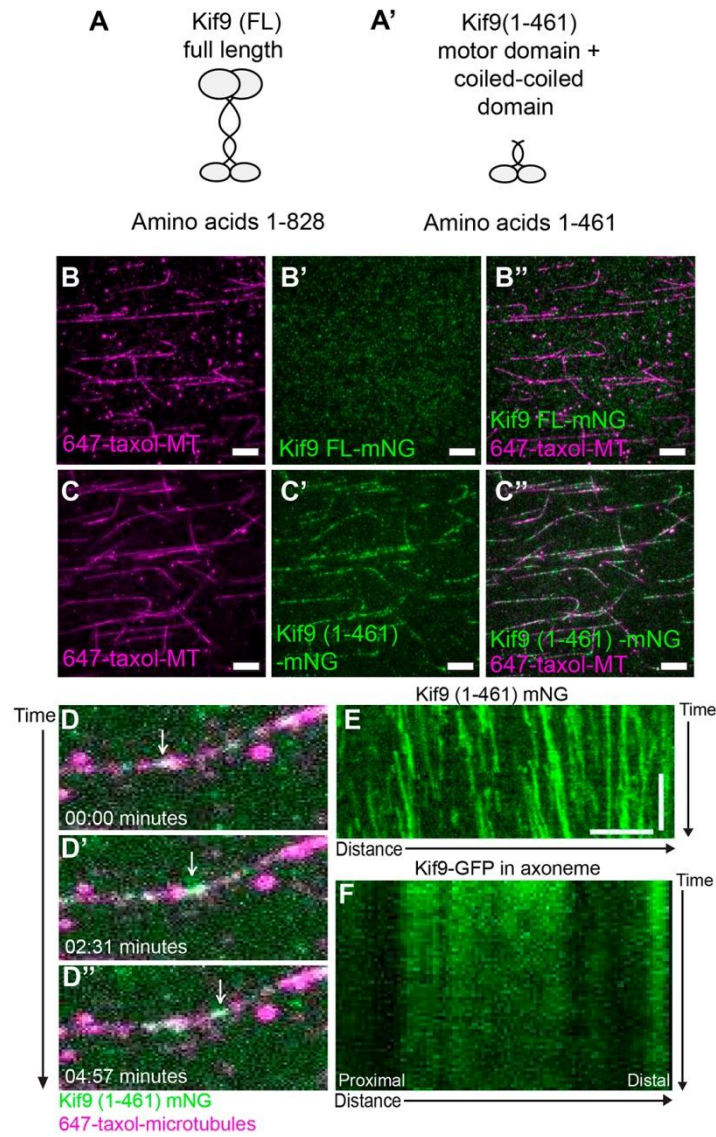


**Figure 7. Motor activity of *Xenopus* Kif9.** A. Schematic of *Xenopus laevis* Kif9 constructs made for single molecule assays. B-B''. Images of single molecule microtubule binding assays for full length Kif9 (Kif9 (FL)) (green) on taxol stabilized microtubules (magenta). All scale bars 10  $\mu\text{m}$ . C-C''. Images of single molecule microtubule binding assays for a truncated version (Kif9 (1-461)) (green) on taxol stabilized microtubules (magenta). All scale bars 10  $\mu\text{m}$ . D-D''. Still frames from live imaging of Kif9 processivity on microtubules in minutes. White arrow follows Kif9 particle (green) movement along microtubule (magenta). E. Kymograph of live imaging of Kif9 (1-461)-mNG *in vitro* on microtubules. Scale bars 2 minutes and 5  $\mu\text{m}$ . F. Kymograph of live imaging of Kif9-GFP construct *in vivo* in *Xenopus laevis* multiciliated cell axonemes.

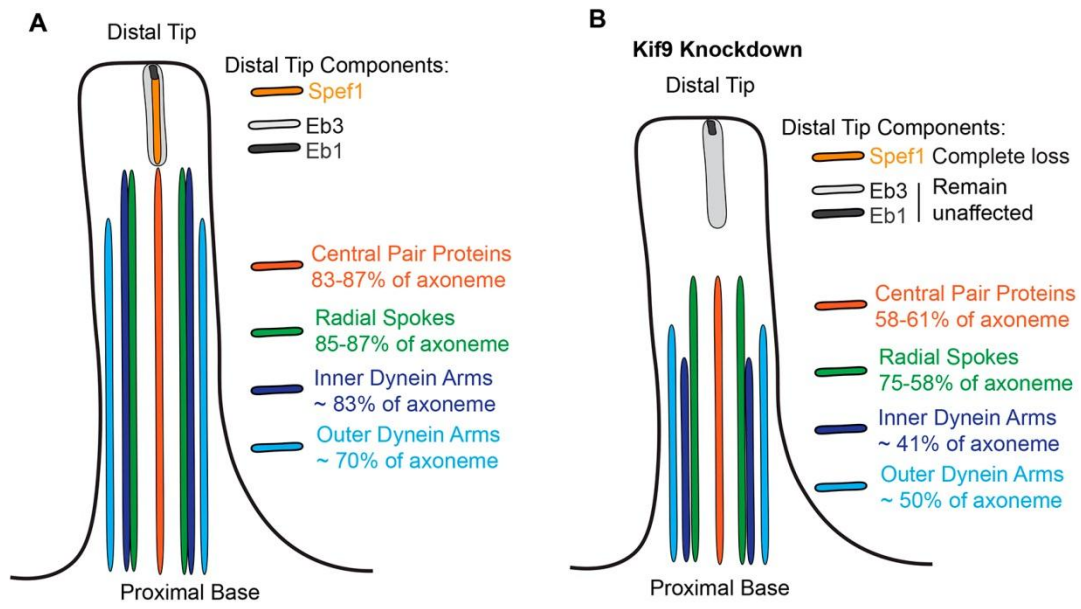


**Figure 8. Summary of effect of Kif9 knockdown on proximal to distal patterning of the motile cilium.** A. Schematic of wildtype motile cilia in *Xenopus* with domains schematized based off findings. B. Schematic of Kif9 knockdown cilia and changes to domains observed.

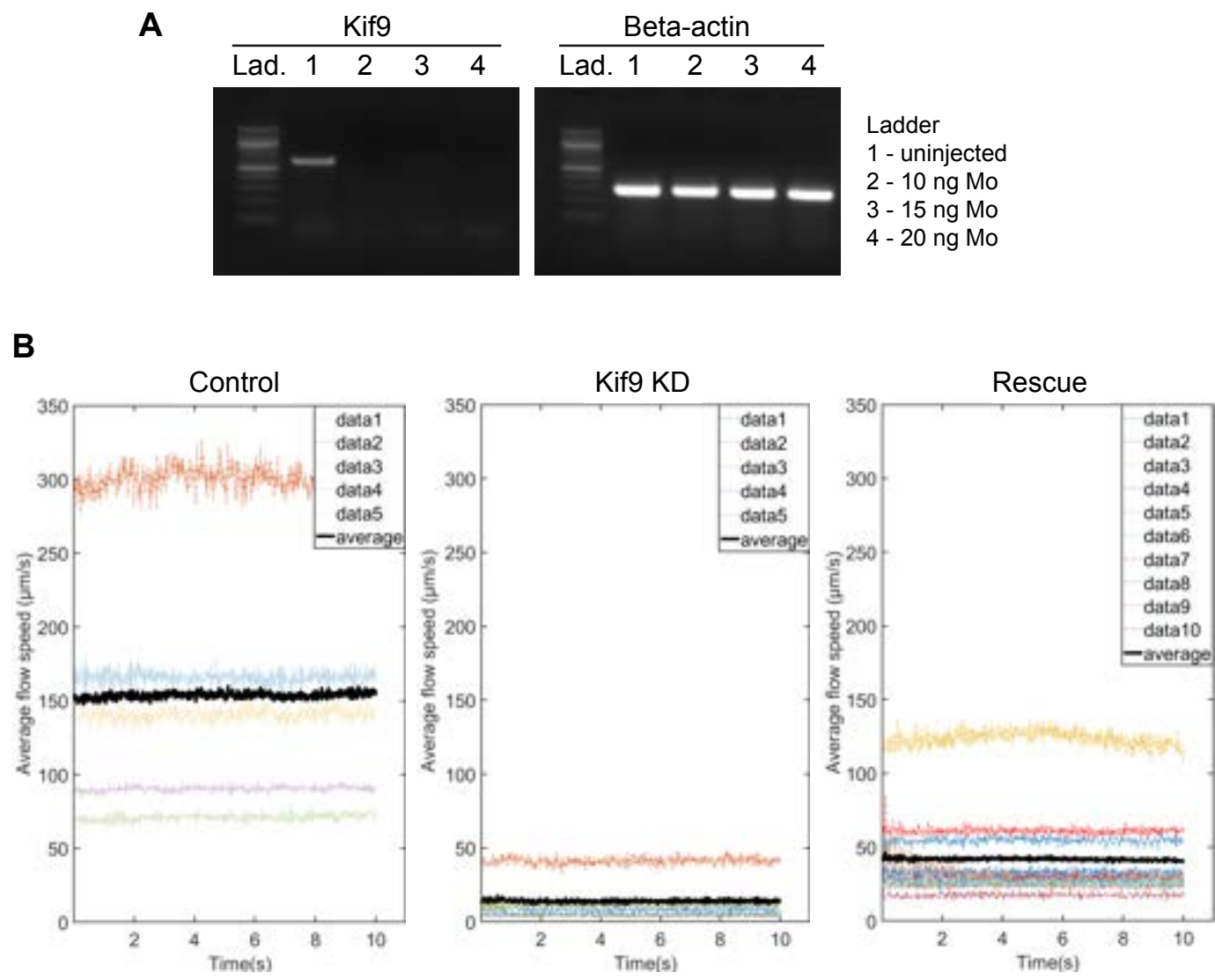


**Fig. S1.** A. Gel image of RT-PCR of Kif9 expression in Kif9 morpholino injected embryos at wildtype, 10 ng, 15 ng, and 20 ng doses. B. Graphs of average bead flow across the epidermis of stage 24 *Xenopus* embryos in Control, Kif9 morpholino, and Rescue injected embryos.

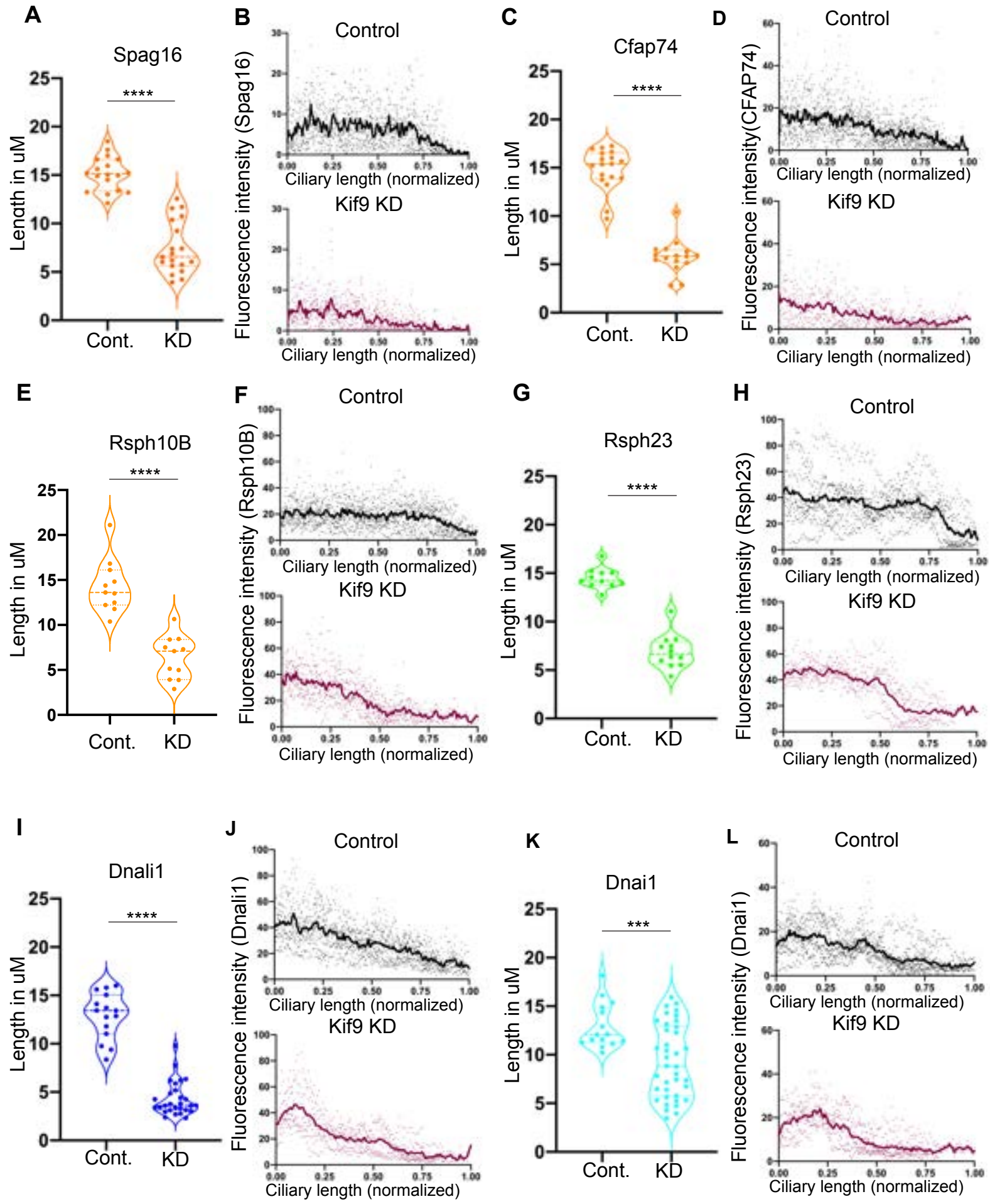


**Fig. S2.** A. Raw quantification of C2 bridge central pair component GFP-Spag16 length in Control and Morpholino injected embryos. B. Graphs of fluorescence intensity of GFP-Spag16 across the length of the cilia, normalized to 1. C. Raw quantification of C1 central pair component GFP-Cfap74 length in Control and Morpholino injected embryos. D. Graphs of fluorescence intensity of GFP-Cfap74 across the length of the cilia, normalized to 1. E. Raw quantification of GFP-Rsph10B length in Control and Morpholino injected embryos. F. Graphs of fluorescence intensity of GFP-Rsph10B across the length of the cilia, normalized to 1. G. Raw quantification of radial spoke stalk component Rsph23 length in Control and Morpholino injected embryos. H. Graphs of fluorescence intensity of GFP-Rsph23 across the length of the cilia, normalized to 1. I. Raw quantification of inner dynein arm GFP-Dnali1 length in Control and Morpholino injected embryos. J. Graphs of fluorescence intensity of GFP-Dnali1 across the length of the cilia, normalized to 1. K. Raw quantification of outer dynein arm GFP-Dnai1 length in Control and Morpholino injected embryos. L. Graphs of fluorescence intensity of GFP-Dnai1 across the length of the cilia, normalized to 1.

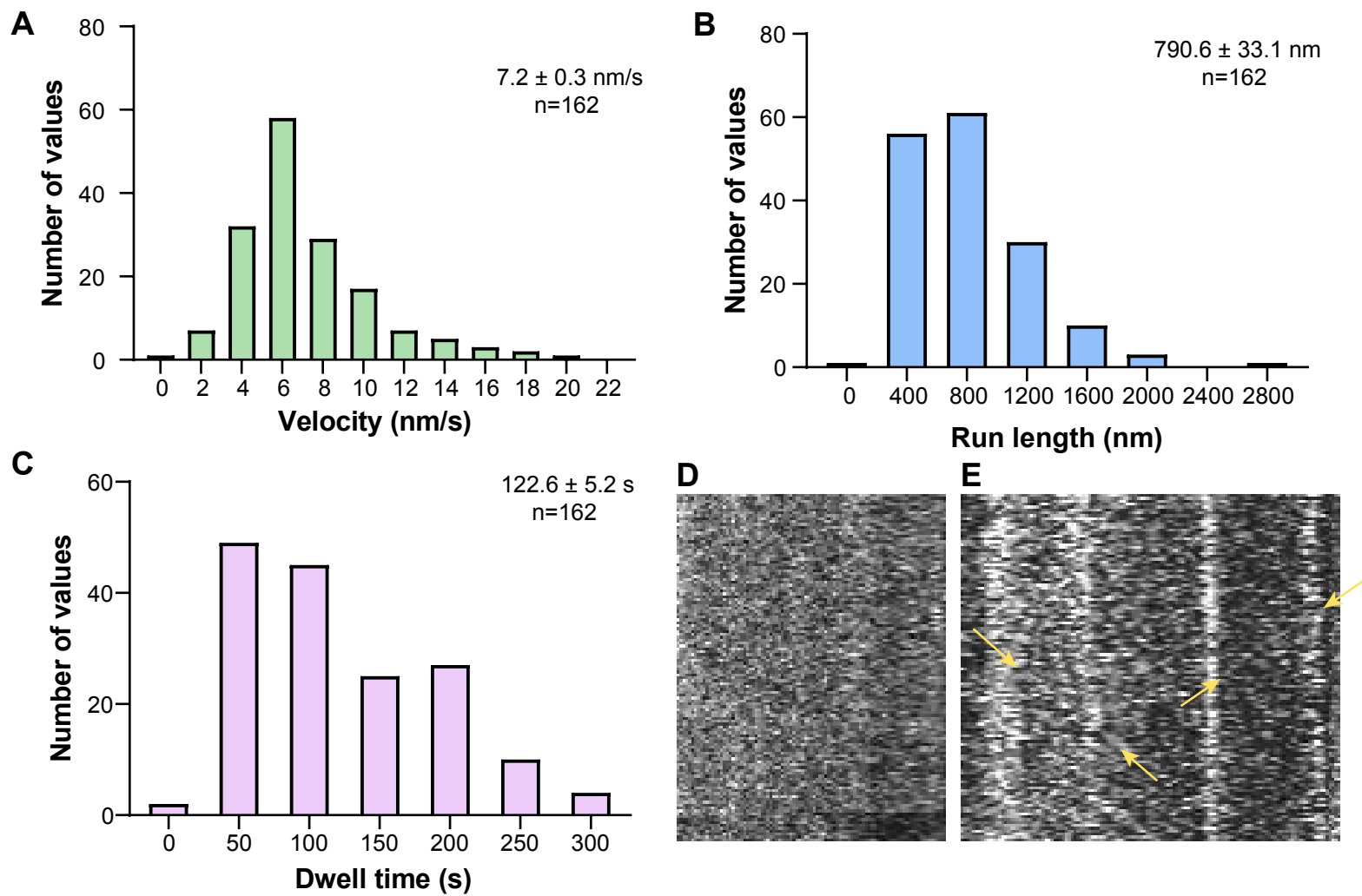
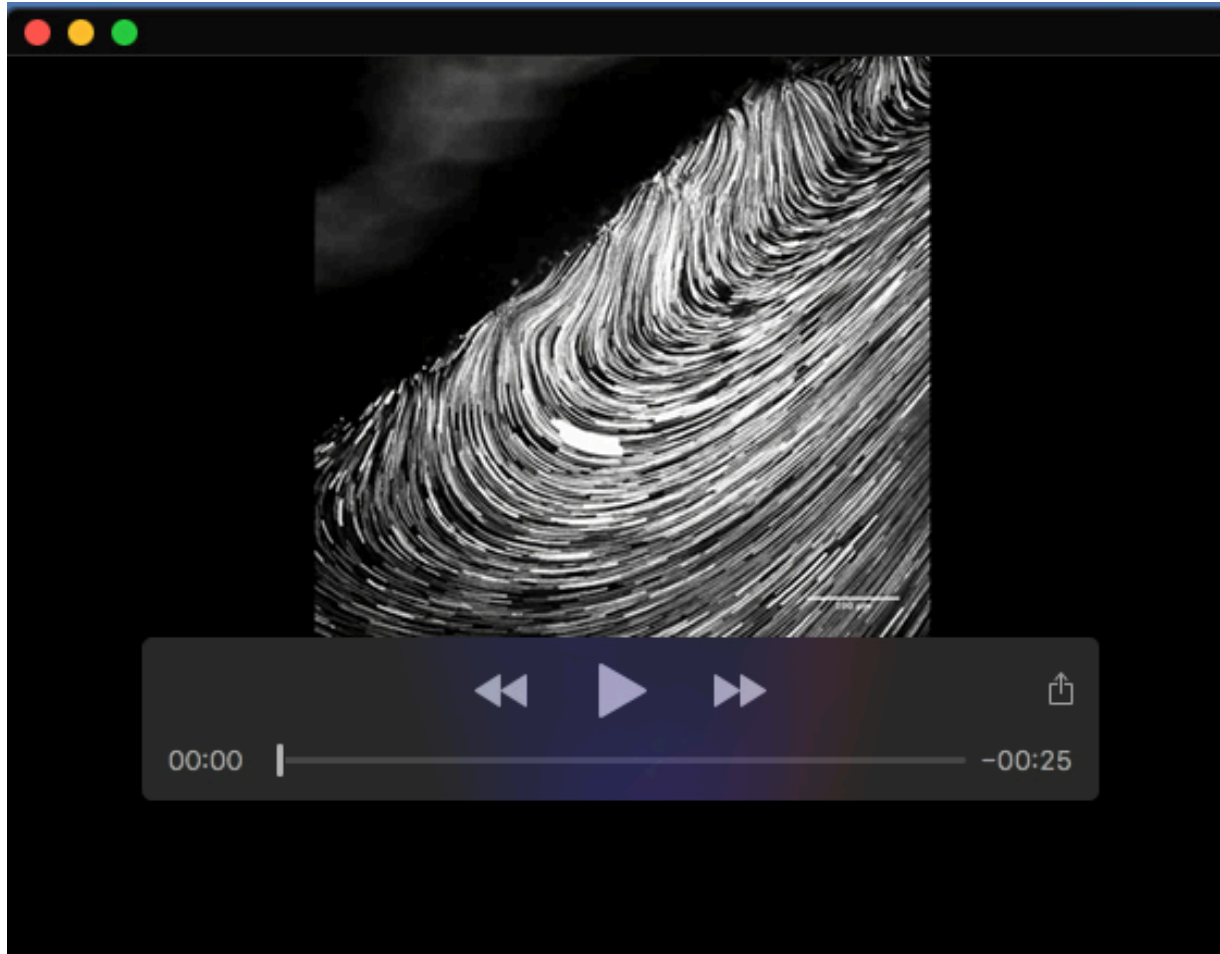
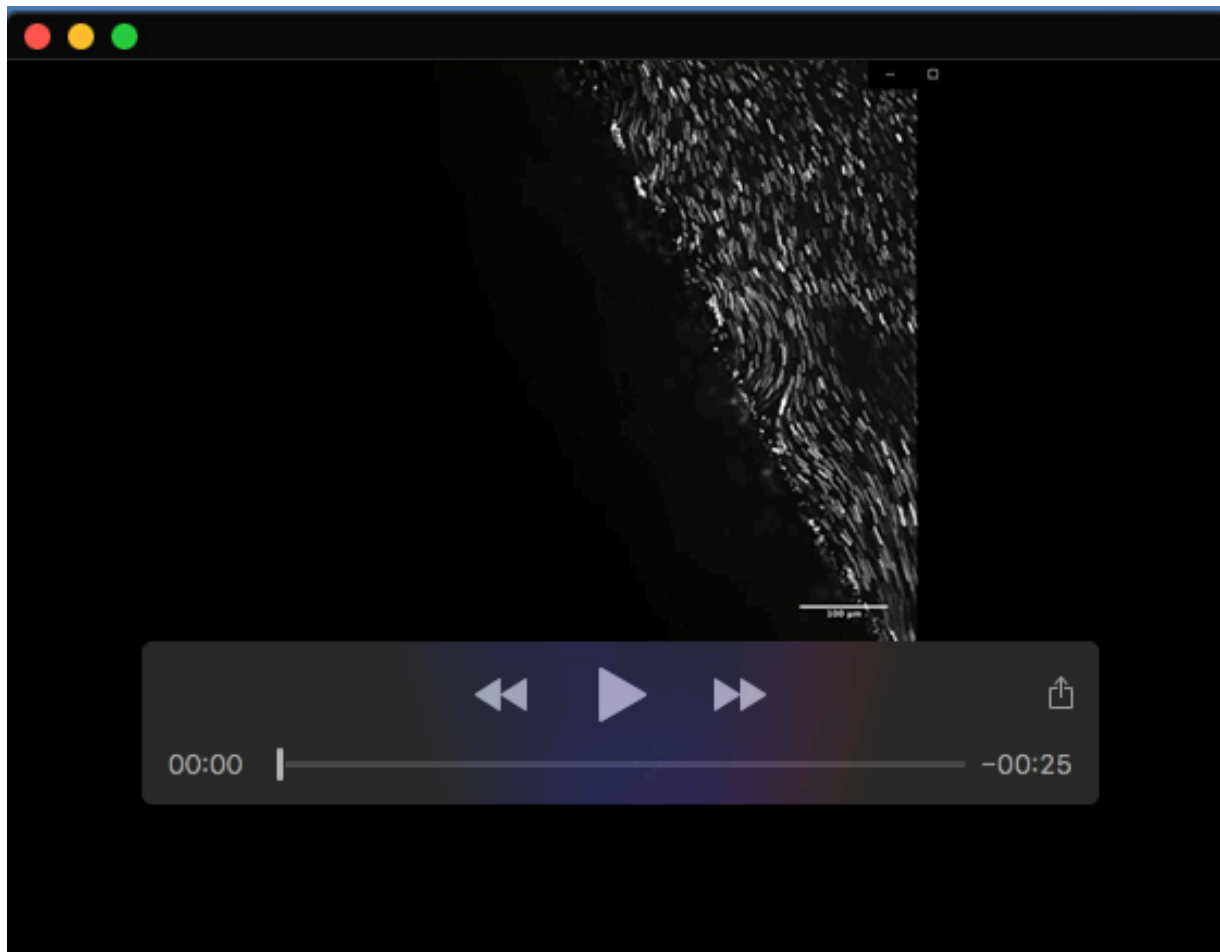


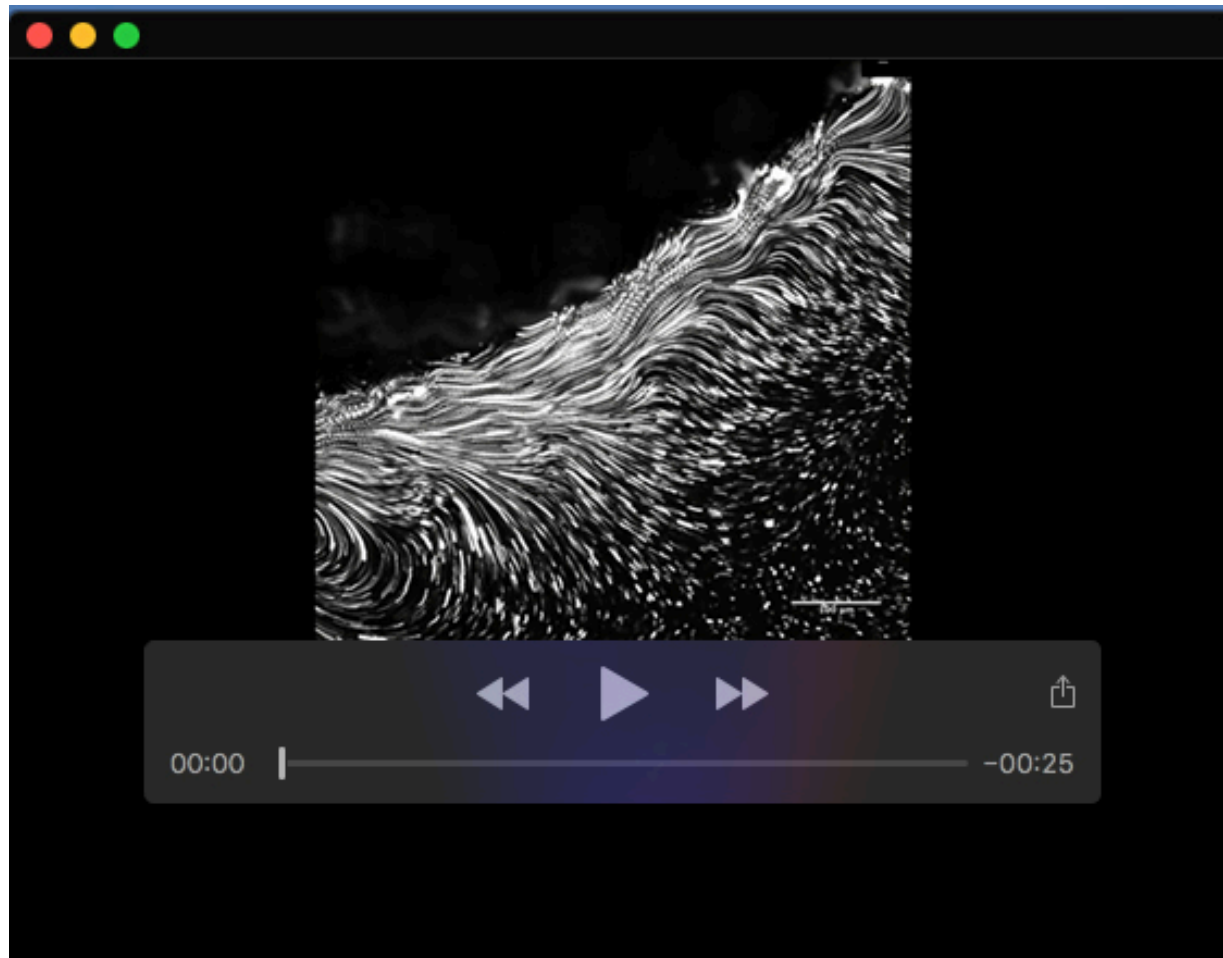
**Fig. S3.** A. Histogram of speed of truncated Kif9 movement along microtubules *in vitro*. Values binned to 1 nanometer/second. X-axis = velocity of molecules in nm/sec. Y-value = number of molecules at given speed. B. Histogram of run length of truncated Kif9 (X-axis) movement and number of molecules tracked (Y-axis). C. Dwell time of paused molecules (X-axis) and number of molecules tracked (Y-axis). D. Kymograph of live imaging of Kif9-GFP in axonemes. E. Kymograph of live imaging of Kif9-GFP in axonemes, arrows pointing to bidirectional trafficking of Kif9-GFP along the axoneme.



**Movie 1. Flowtrace movies of beads flowing past epidermis in control embryos.** Frame rate of 80 frames/second.



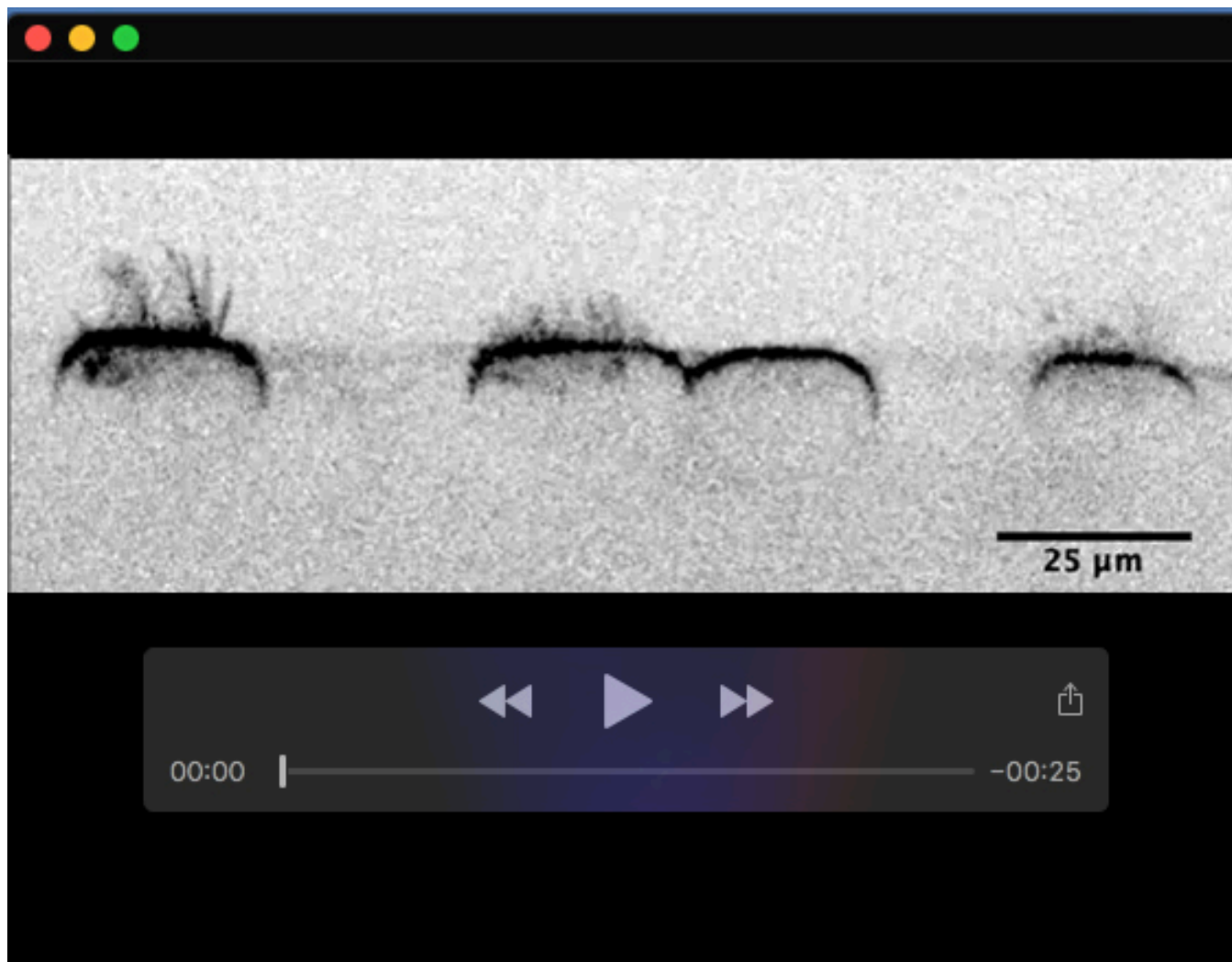
**Movie 2. Flowtrace movies of beads flowing past epidermis in Kif9 knockdown embryos.** Frame rate of 80 frames/second.



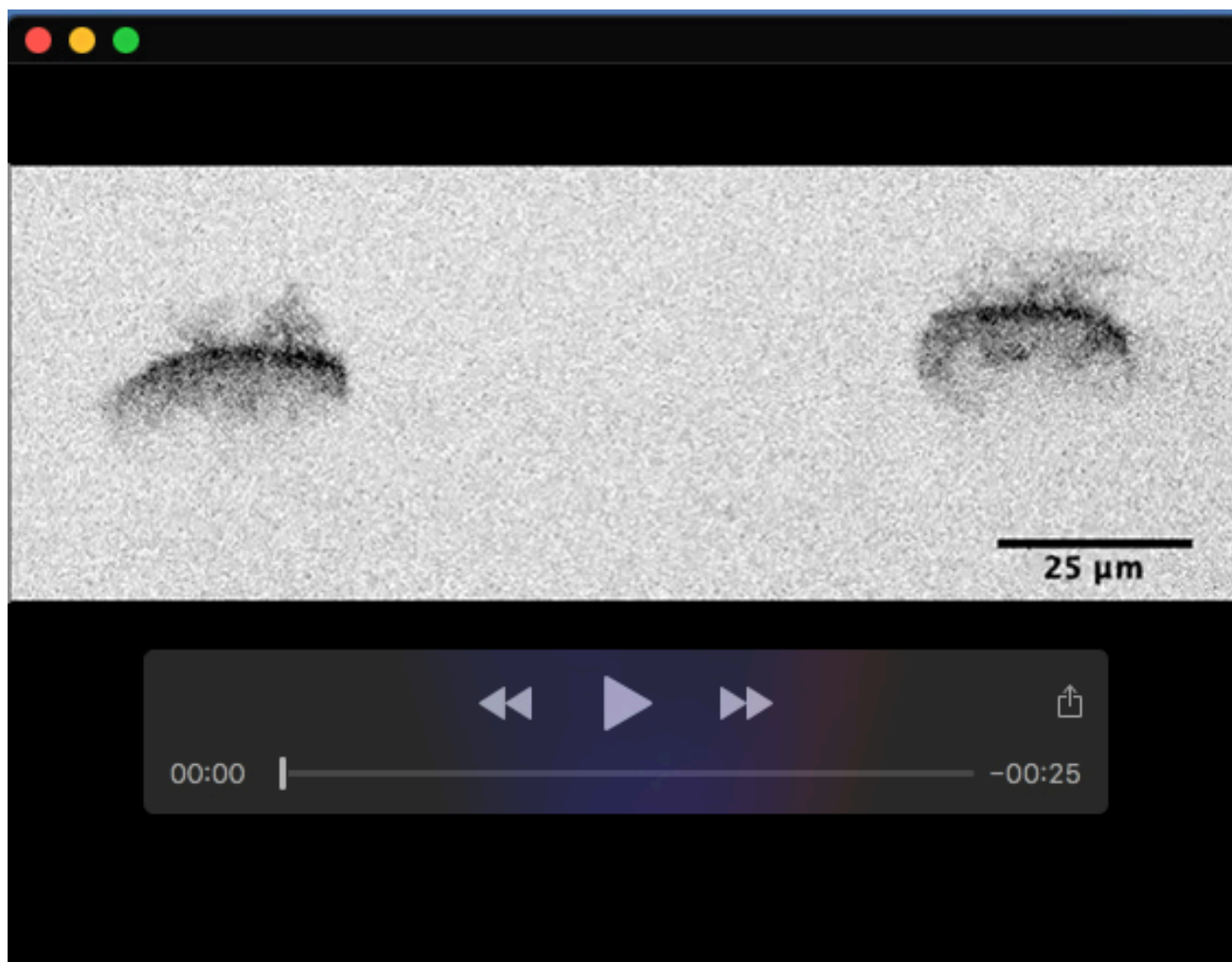
**Movie 3. Flowtrace movies of beads flowing past epidermis in rescue treated embryos.** Frame rate of 80 frames/second.



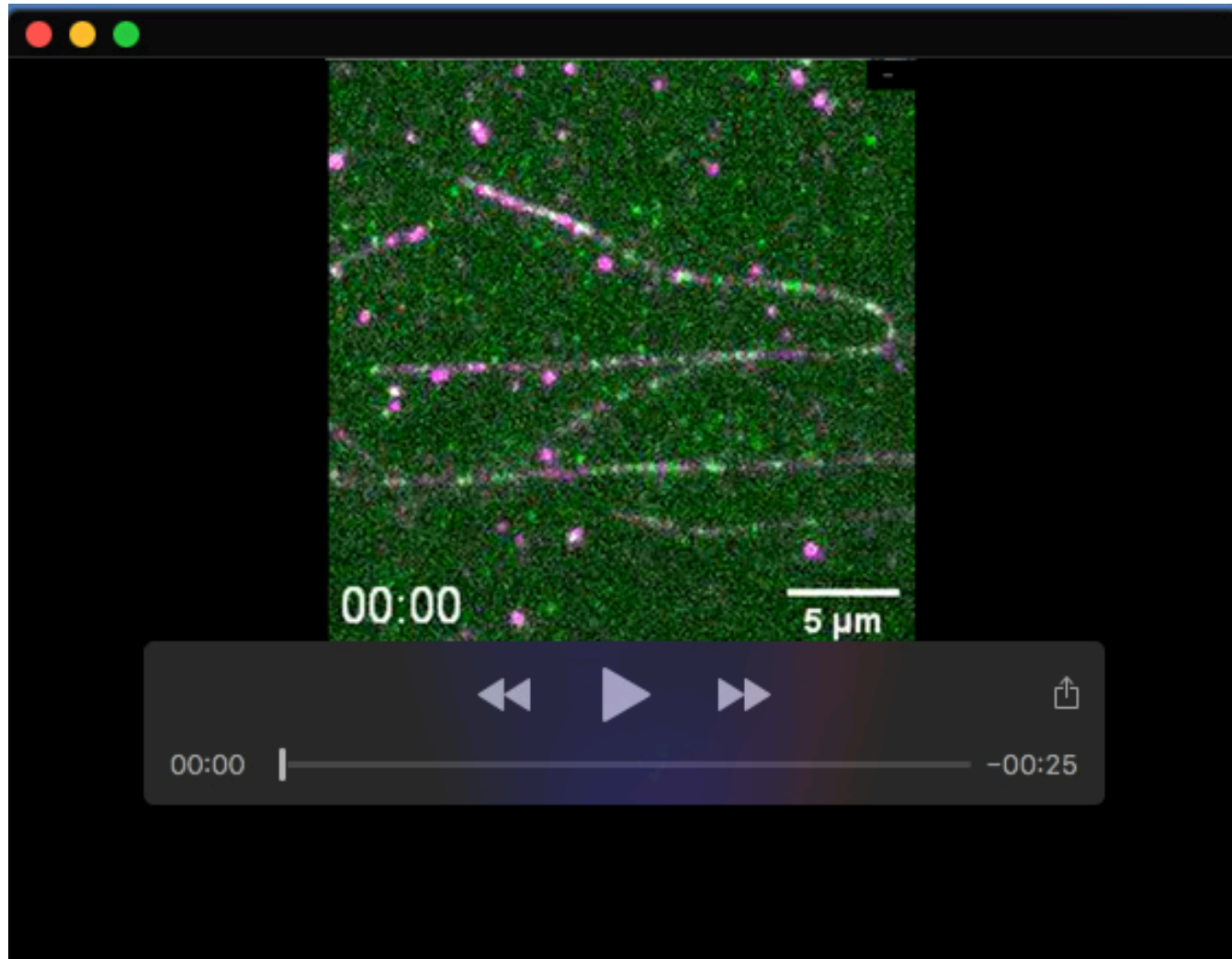
**Movie 4. Multiciliated cell beating in control embryos.** Frame rate of 80 frames/second.



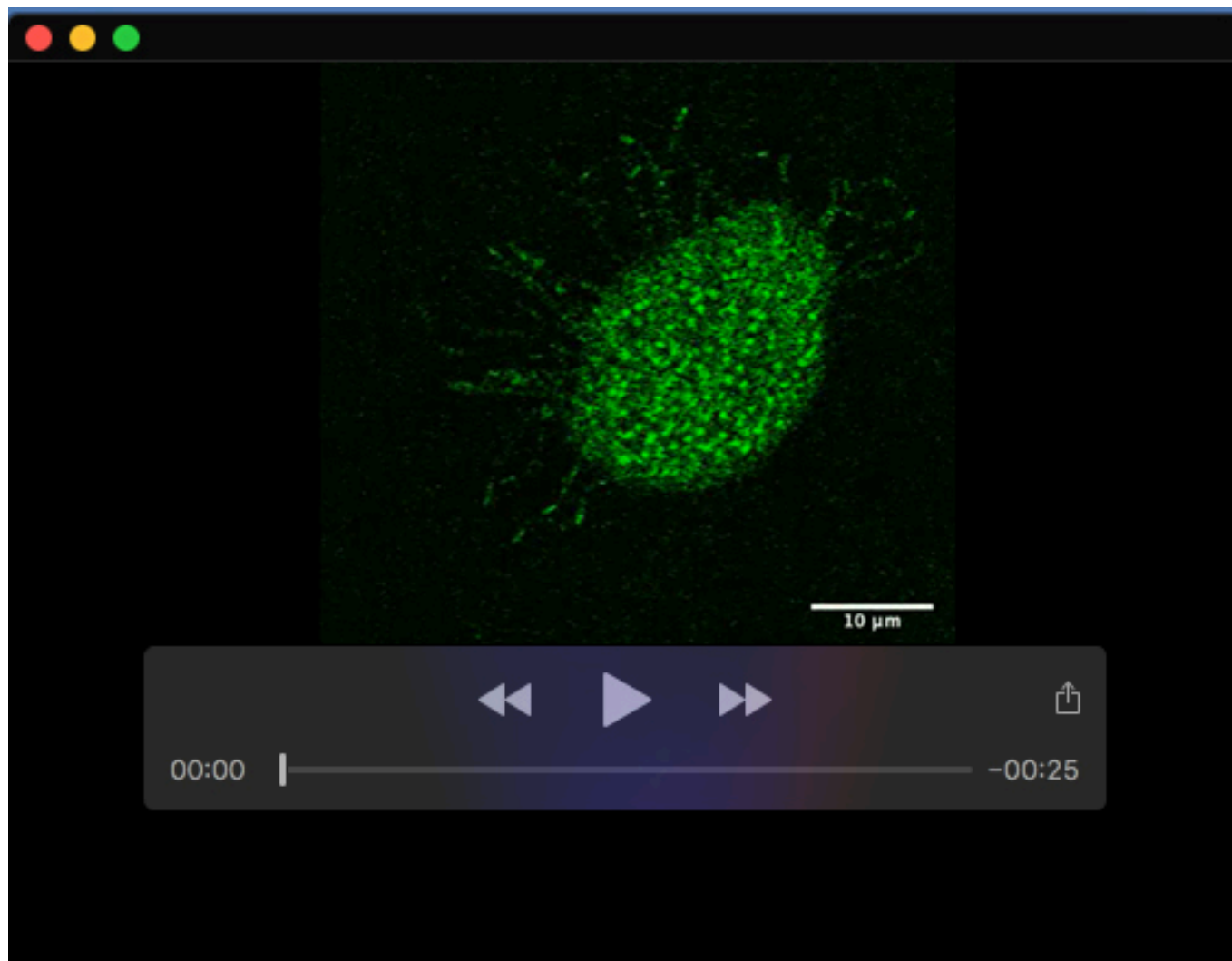
**Movie 5. Multiciliated cell beating in Kif9 knockdown embryos.** Frame rate of 80 frames/second.



**Movie 6. Multiciliated cell beating in rescue treated embryos.** Frame rate of 80 frames/second.



**Movie 7.** Movie of truncated version of Kif9 (Kif9 1-461 mNG) migrating on microtubules. Frame rate of 3 seconds/frame.



**Movie 8.** Movie of Kif9-GFP in vivo in *Xenopus* multiciliated cells. Frame rate of 3.84 frames/second.